The Abdus Salam
International Centre
for Theoretical Physics

2359-22

Joint ICTP-IAEA Workshop on Physics of Radiation Effect and its Simulation for Non-Metallic Condensed Matter

13 - 24 August 2012

Swift heavy ion irradiation of nanostructured materials

V.A. Skuratov

Joint Institute for Nuclear Research
Dubna
Russia

Swift heavy ion irradiation of nanostructured materials

V.A.Skuratov

Flerov Laboratory of Nuclear Reactions
Joint Institute for Nuclear Research, Dubna, Russia

Outline

- **Formation of nanostructures on the surface of radiation-resistant insulators by single high energy ions**
- **Modification of Si nanocrystallites in SiO_2 matrix by swift heavy ion irradiation**
- **Radiation stability of nanocrystalline ceramics irradiated with high-energy ions**
- **Oxide nanoparticles in the ODS alloys irradiated with swift heavy ions**

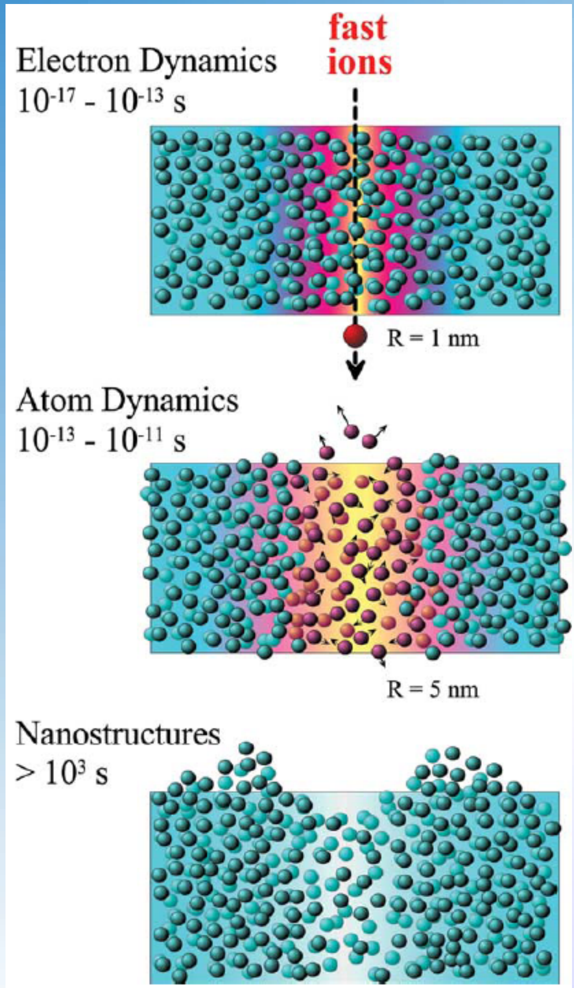

The source of structural changes in tracks of high energy (E > 1 MeV/amu) heavy ions is a huge energy deposition (tens keV/nm) in electron subsystem of irradiating material

Nanostructuring may enhance localization of energy deposition in the ion trajectory region and affect the latent track formation process

G. Schiwietz et al. NIMB 226 (2004) 683

Sapphire surface irradiated with 10^{10} C_{60}^{2+} cm^{-2} at normal incidence

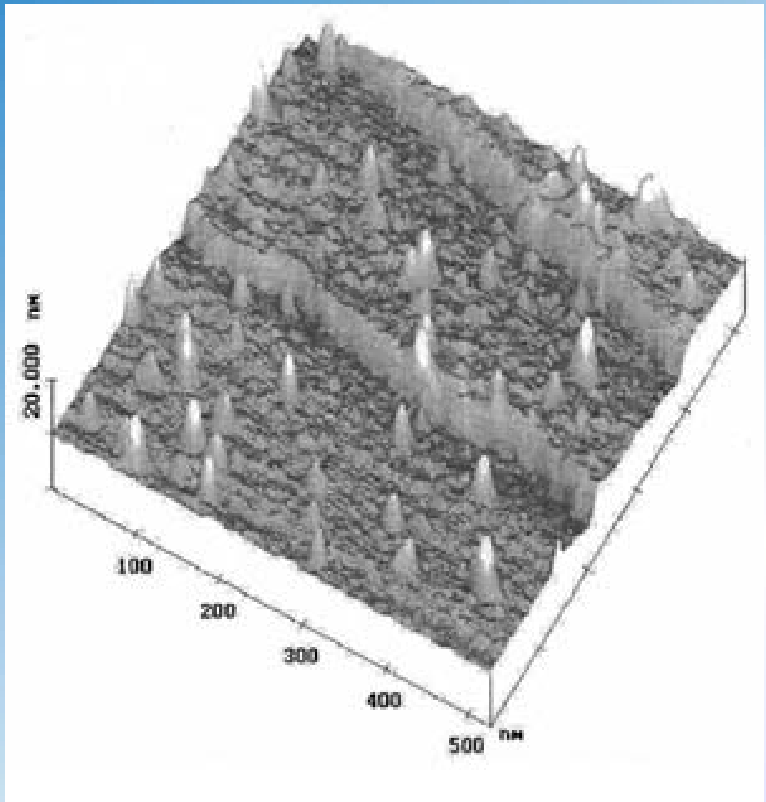

E=30 MeV, S_e=76.2 keV/nm, mean hillock height – 4.5±0.5 nm.

The hillock structures result from an out of plane expansion of the amorphous core tracks related to a relative decrease in the density of amorphized α-Al_2O_3.

Ramos S. M. M. et. al. Nucl. Instr. Meth., 1998, B143, p. 319-332

3D AFM image of of $MgAl_2O_4$ surface irradiated with 710 MeV Bi ions.
Ion fluence $5x10^{10}$ cm^{-2}.

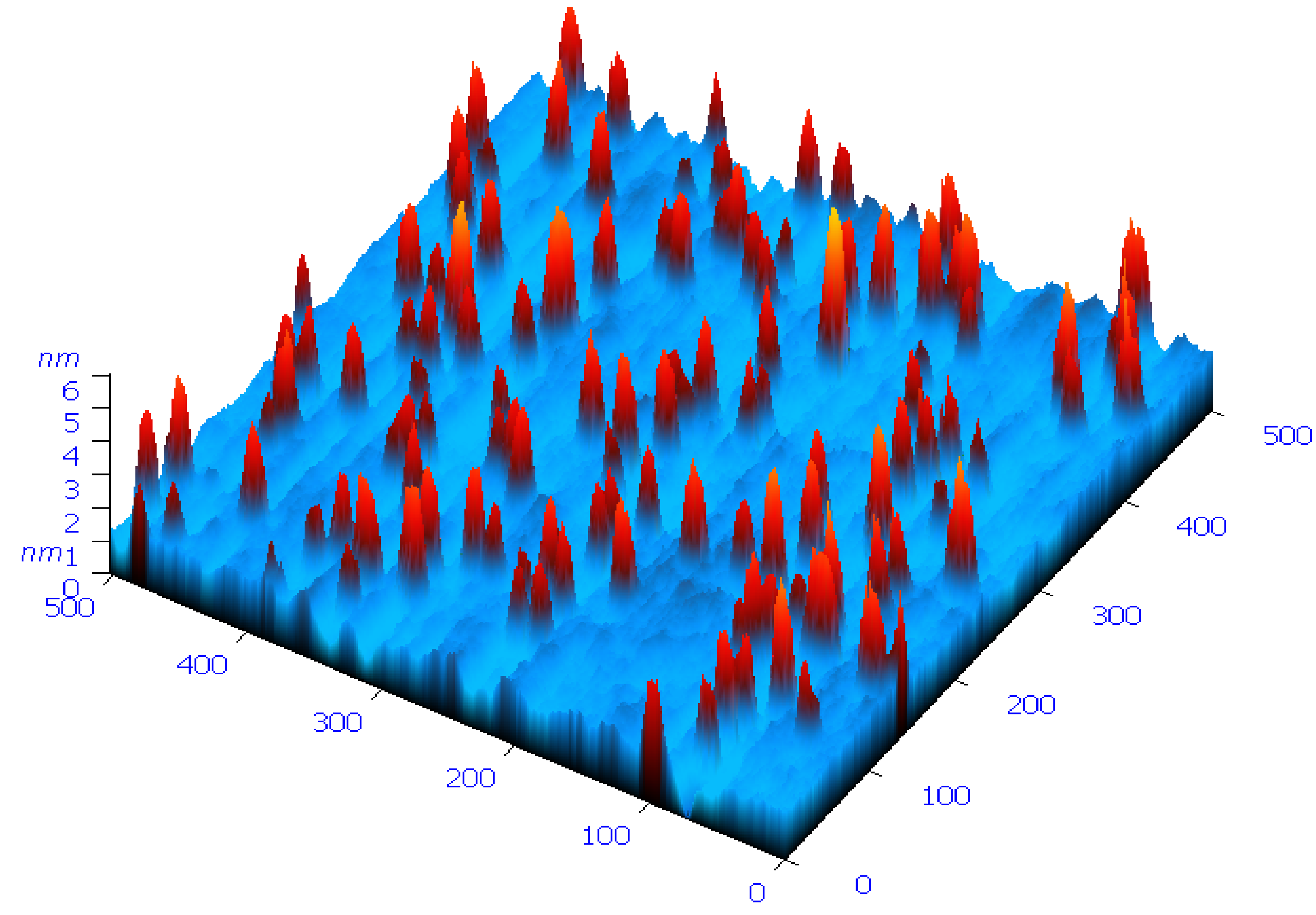

2D AFM image of spinel surface irradiated with 580 MeV Xe ions

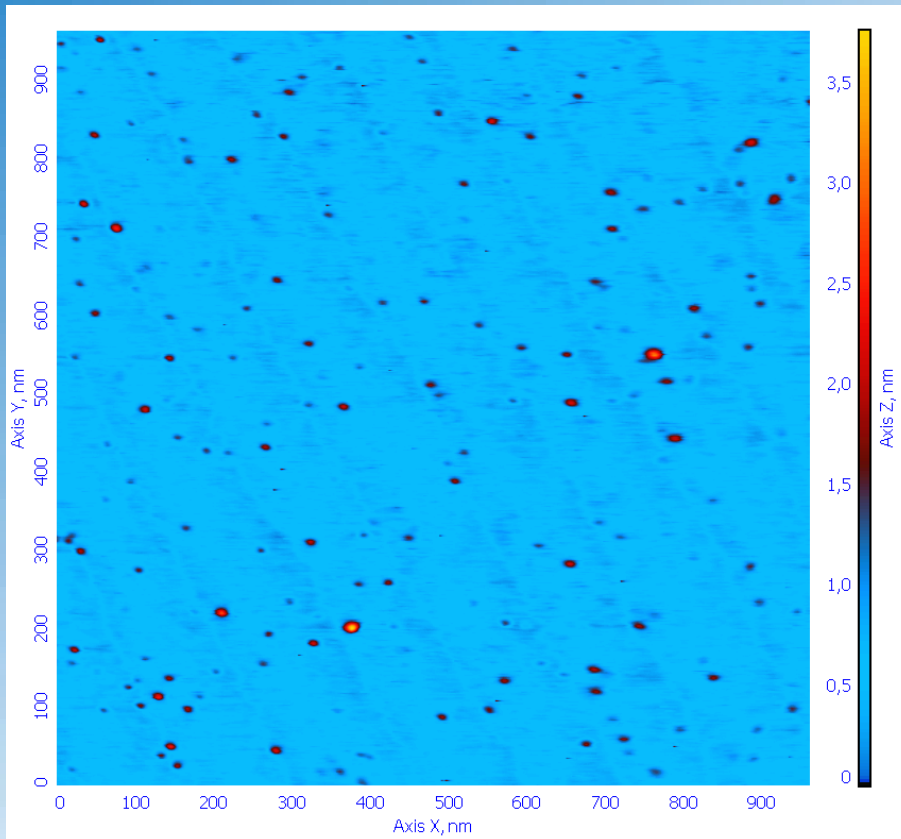

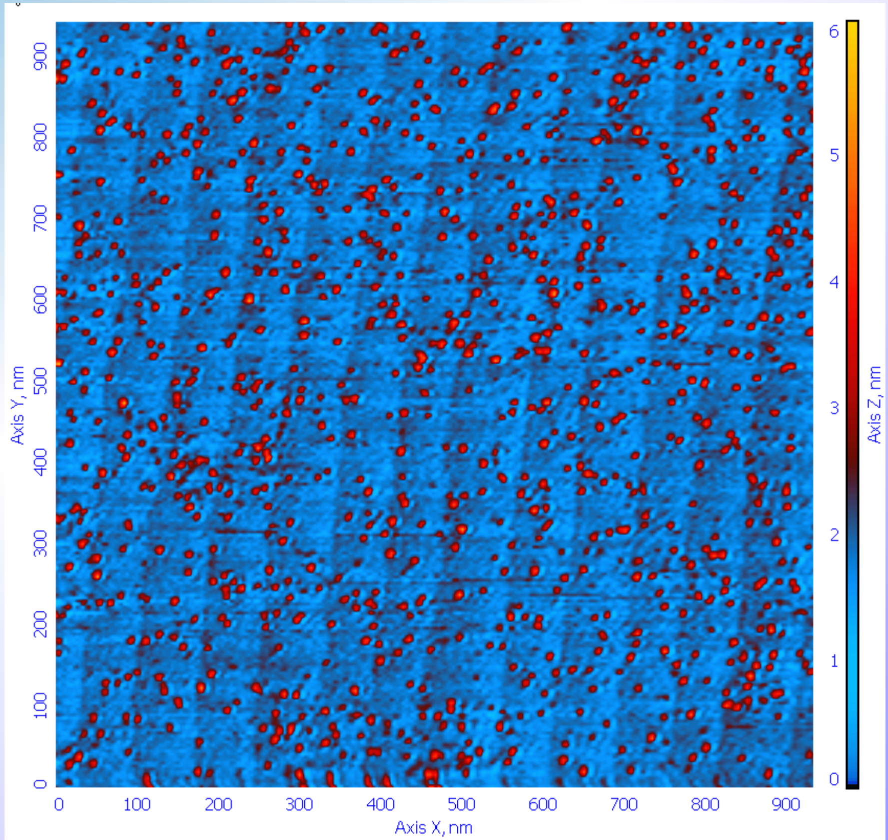

$\Phi t = 2 \times 10^{10}\ cm^{-2}$

Number of hillocks: $1.87 \times 10^{10}\ cm^{-2}$

$\Phi t = 1 \times 10^{11}\ cm^{-2}$

Number of hillocks: $0.91 \times 10^{11}\ cm^{-2}$

3D AFM images of α-A_2O_3 surface irradiated with 5×10^{10} cm^{-2} Bi ions of different energies

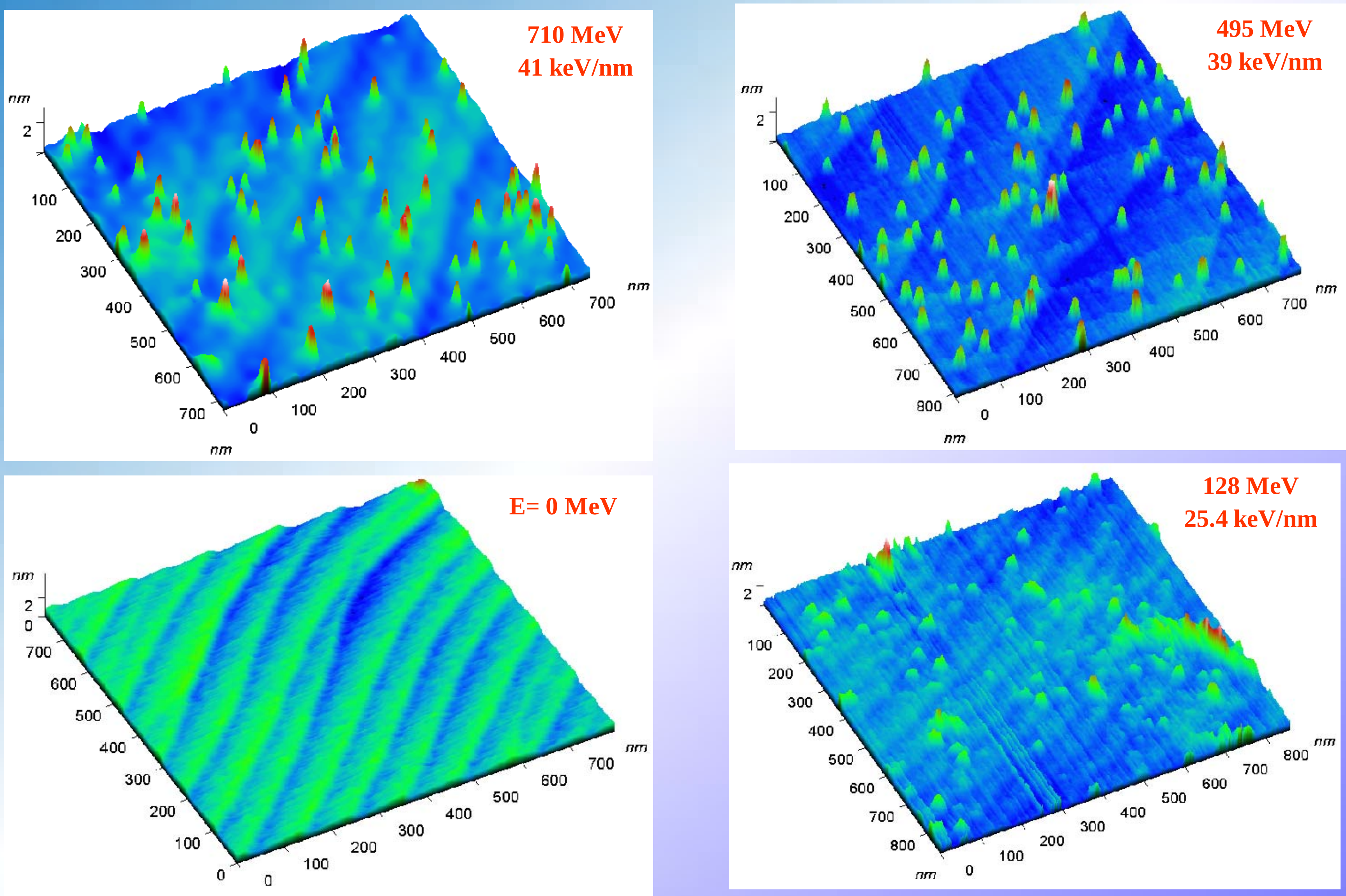

Surface effects of dense ionization in radiation-resistant insulators

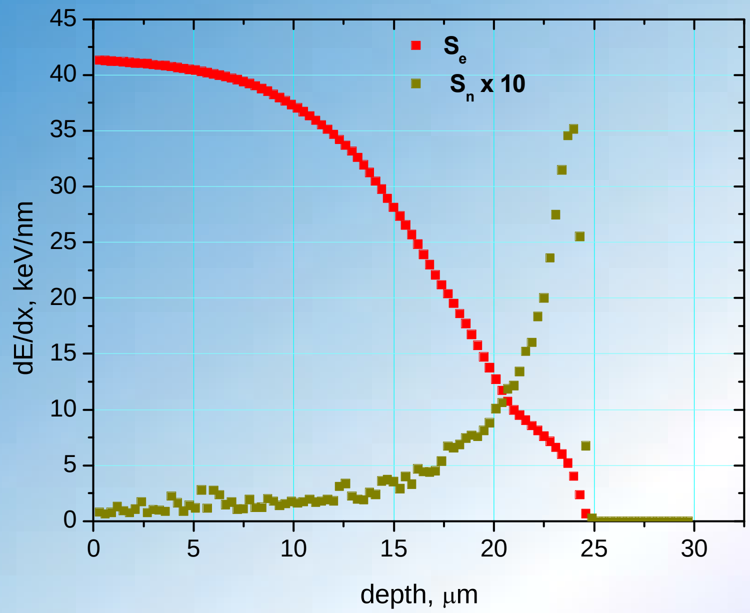

Calculated electronic (S_e) and nuclear (S_n) stopping powers of 710 MeV Bi ions in sapphire

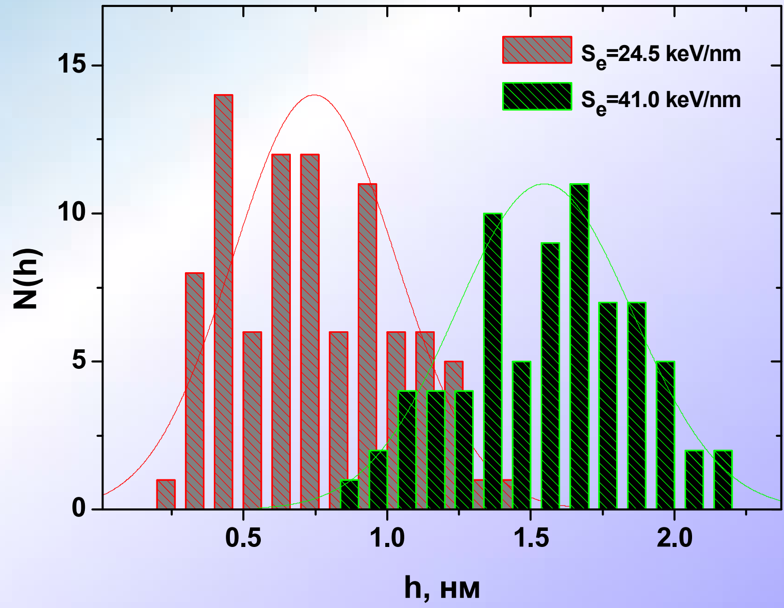

Distribution of the hillock heights in sapphire for 128 and 710 MeV Bi ions

- **The projectile ions produce nanoscale hillock-like surface defects above a certain threshold energy**
- **These defects have inelastic collision (electronic stopping) origin**

Ion irradiation parameters

Ion type	Energy, MeV	target	S_e, kev/nm	Ion fluence, cm^{-2}	$T_{irr.}$, K	α, degr.
Bi^{+51} Bi^{+32} Bi^{+25} Bi^{+17}	710 495 292 128	Al_2O_3	41 39 36 25,4	2×10^{10}, 10^{11} 5×10^{11}, 10^{12}	77, 300	0, 30, 45, 60, 75
Bi^{+51}	710	MgO	38,1	2×10^{10}	300	0
Bi^{+51}	710	$MgAl_2O_4$	36,7	-	-	-
Bi^{+51}	710	SiC	34	-	-	-
Bi^{+51}	710	YSZ	43	2×10^{10}, 5×10^{10}	-	-
W^{+32}	180	$MgAl_2O_4$	25,2	5×10^{10}, 10^{11}	300, 1000	-
W^{+32}	180	Al_2O_3	27	-	300	-
W^{+32}	180	YSZ	28,9	-	-	-
Xe^{+38}	580	Al_2O_3	28,6	2×10^{10}, 10^{11}	-	-
Xe^{+38}	580	$MgAl_2O_4$	25,9	-	-	-
Xe^{+38}	580	YSZ	30	-	-	-
Xe^{+37}	430	YSZ	30,5	2×10^{10}		-
Xe^{+31}	233	YSZ	29	-		-
Xe^{+31}	233	$MgAl_2O_4$	24,4	-	-	-
Xe^{+31}	233	Al_2O_3	26,6	-	-	-
Xe^{+23}	130	$MgAl_2O_4$	21,5	-	-	-
Xe^{+23}	130	YSZ	24,4			-
Xe^{+23}	130	Al_2O_3	23	-	-	-
Kr^{+27}	305	Al_2O_3	16,6	-	-	-
Kr^{+27}	245	Al_2O_3	16,8	-	-	-
Kr^{+27}	245	MgO	15,8	-	-	-
Kr^{+27}	245	$MgAl_2O_4$	15,5	-	-	-
Kr^{+15}	85	$MgAl_2O_4$	14,6	-	-	-

Variation of the mean hillock height with incident electronic stopping power

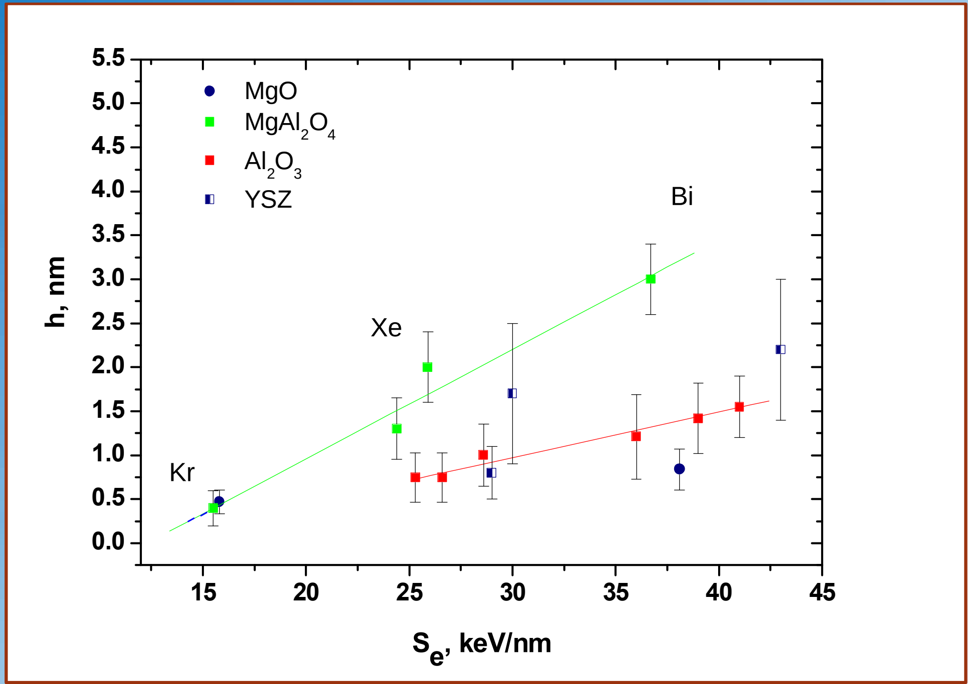

Correlation between the mean hillocks height and threshold electronic stopping power required for the lattice disorder in the bulk material

the hillocks are higher in $MgAl_2O_4$, having a lower threshold level

$MgAl_2O_4$ - S_e = 8 keV/nm

Al_2O_3 - S_e = 20 keV/nm

MgO - Se = ?

SiC - S_e > 34 keV/nm

MgO Electronic sputtering yield for magnesium oxide at S_e = 15 keV/nm is 4 times less in comparison with sapphire (*N. Matsunami, M. Sataka, A. Iwase, S. Okayasu, NIM B 209 (2003) 288.)*

A_2O_3 surface relief evolution with 710 MeV Bi ion fluence

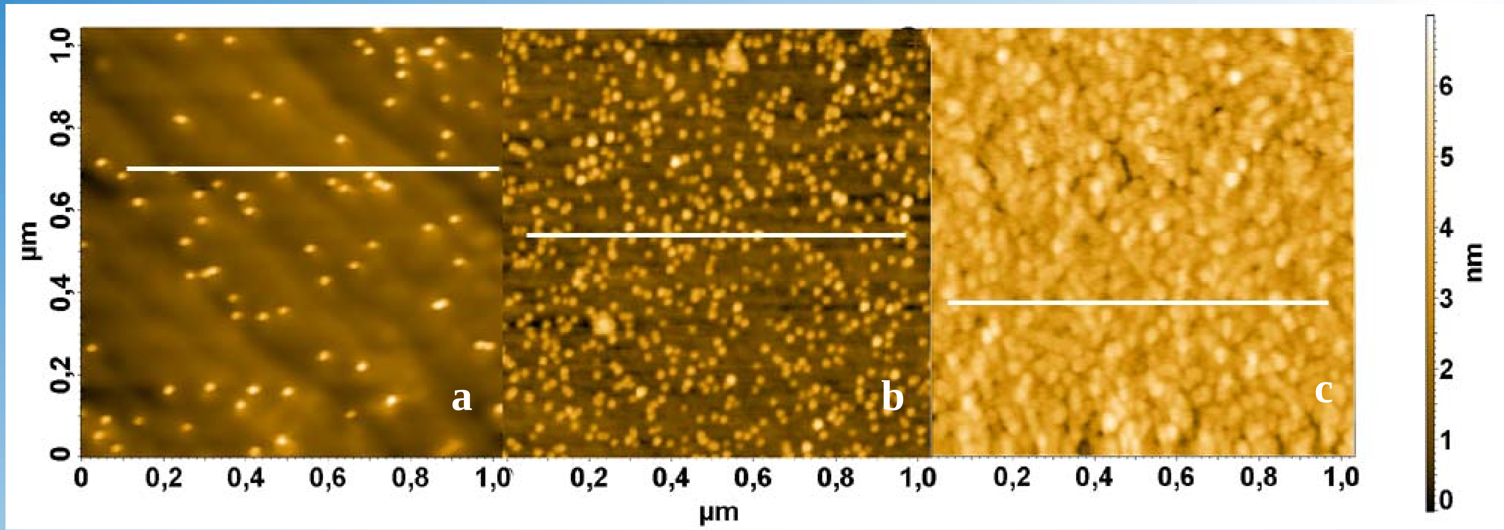

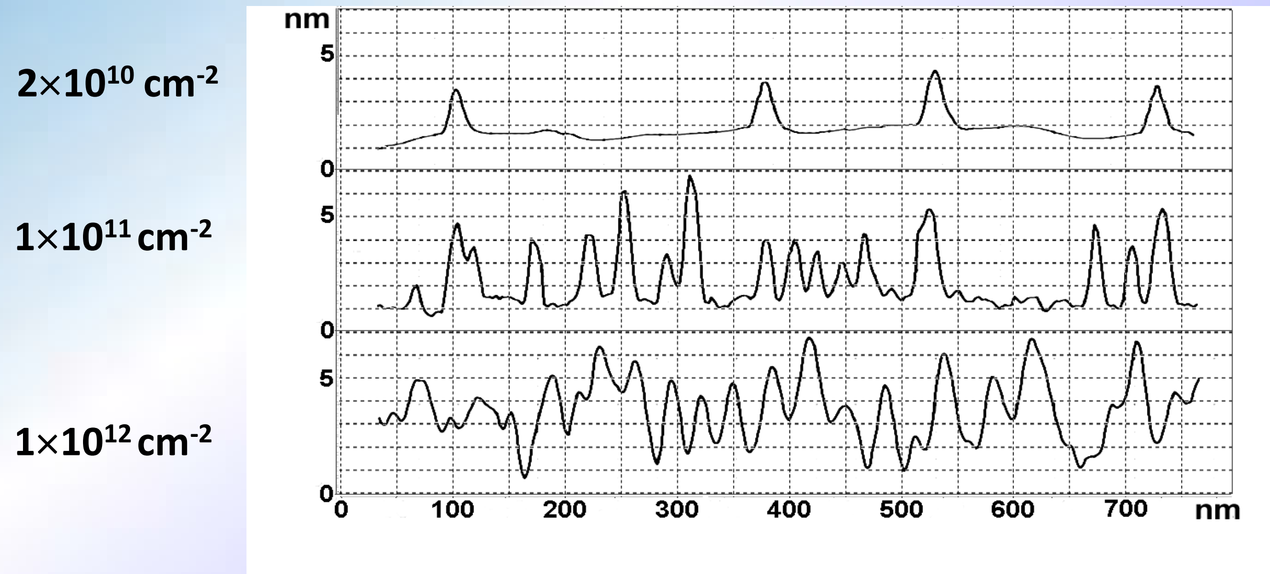

Variation of the hillock shape on Al_2O_3 with Bi ion beam incidence angle

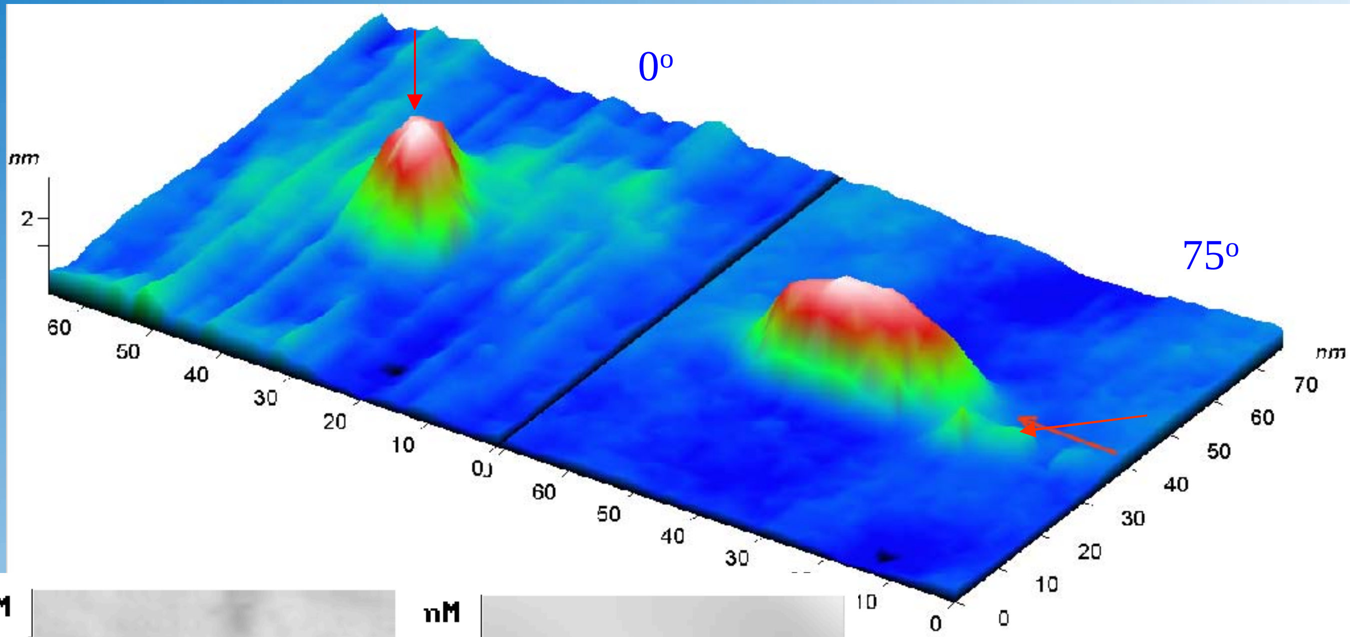

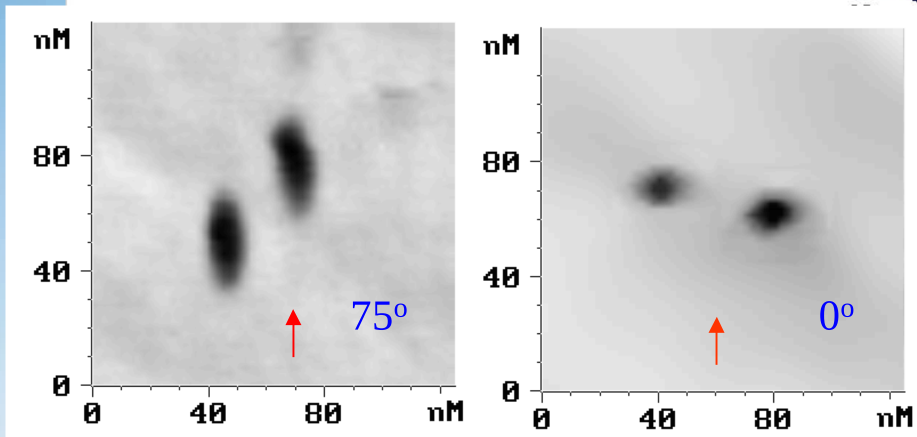

AFM phase images of α-A_2O_3 surfaces irradiated with 710 MeV Bi ions. The arrows show the ion beam direction

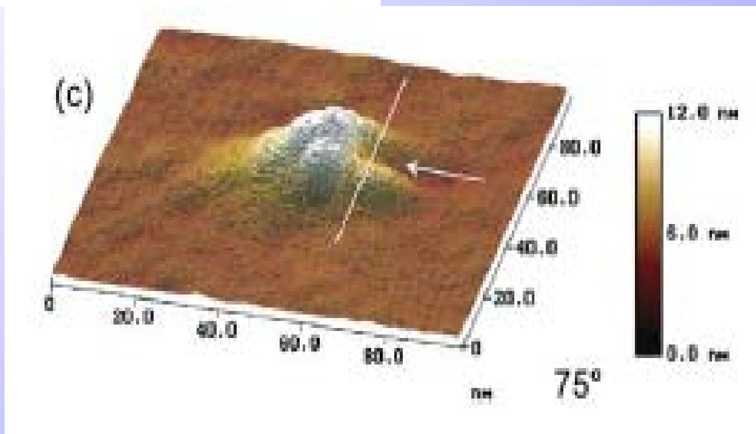

30 MeV C_{60} + $Fe_{0:55}Zr_{0:45}$ alloys

J.C. Girard et. al. Nucl. Instr. Meth., B 209 (2003) 85 .

3D AFM images of of α-A_2O_3 surfaces irradiated at 80K and 300K

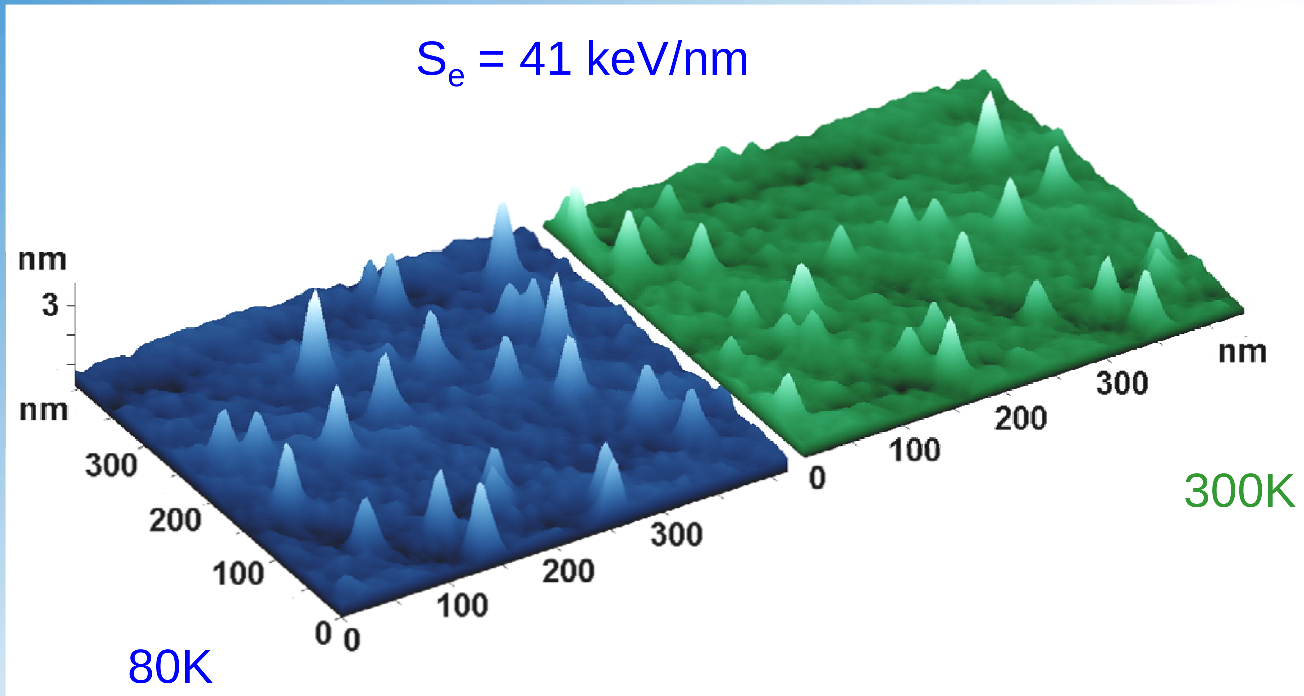

Thermal conductivity of sapphire: 1100 W/mK (80 K)

30-40 W/mK (300 K)

Mechanisms of the hillock-like damage formation

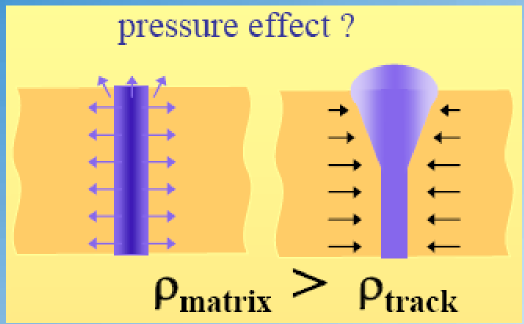

C.Trautman (International school on Radiation Effects in Solids, Erice, Italy, July 2004)

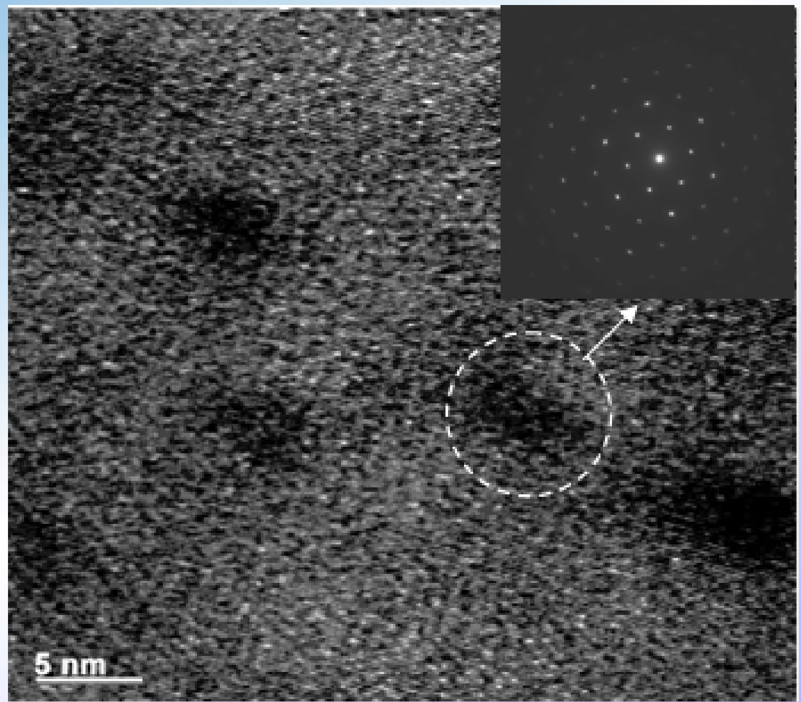

High-resolution lattice image of α-A_2O_3 irradiated with 710 MeV Bi ions to a fluence of 7×10^{12} cm^{-2} at room temperature (plan-view specimen). The average TEM track diameter is ~3 to 4 nm. **Direct track amorphization is not observed**

Mechanisms of the hillock-like damage formation

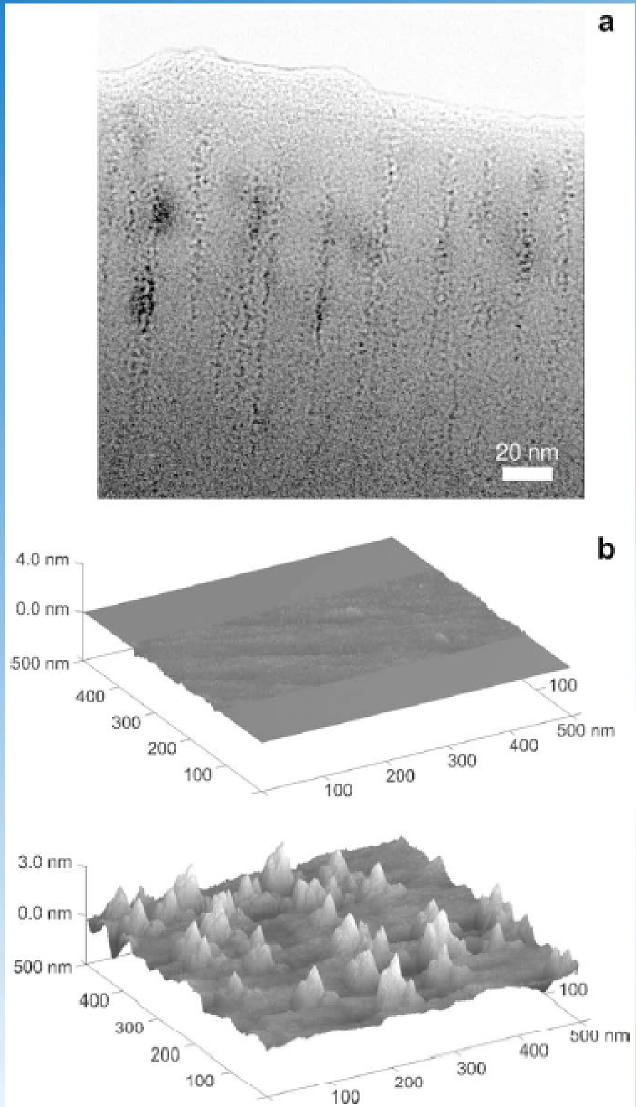

Cross-sectional TEM micrograph of the near-surface region of an YSZ single crystal irradiated with 940 MeV Pb ions at a fluence of 5 10^{11} cm^{-2} (ion tracks are empty of matter)

AFM micrograph of the surface of an YSZ single crystal before (virgin) and after irradiation with 940 MeV Pb ions at a fluence of 10^{10} cm^{-2}.

S. Moll et al./ Vacuum 83 (2009) S61–S64

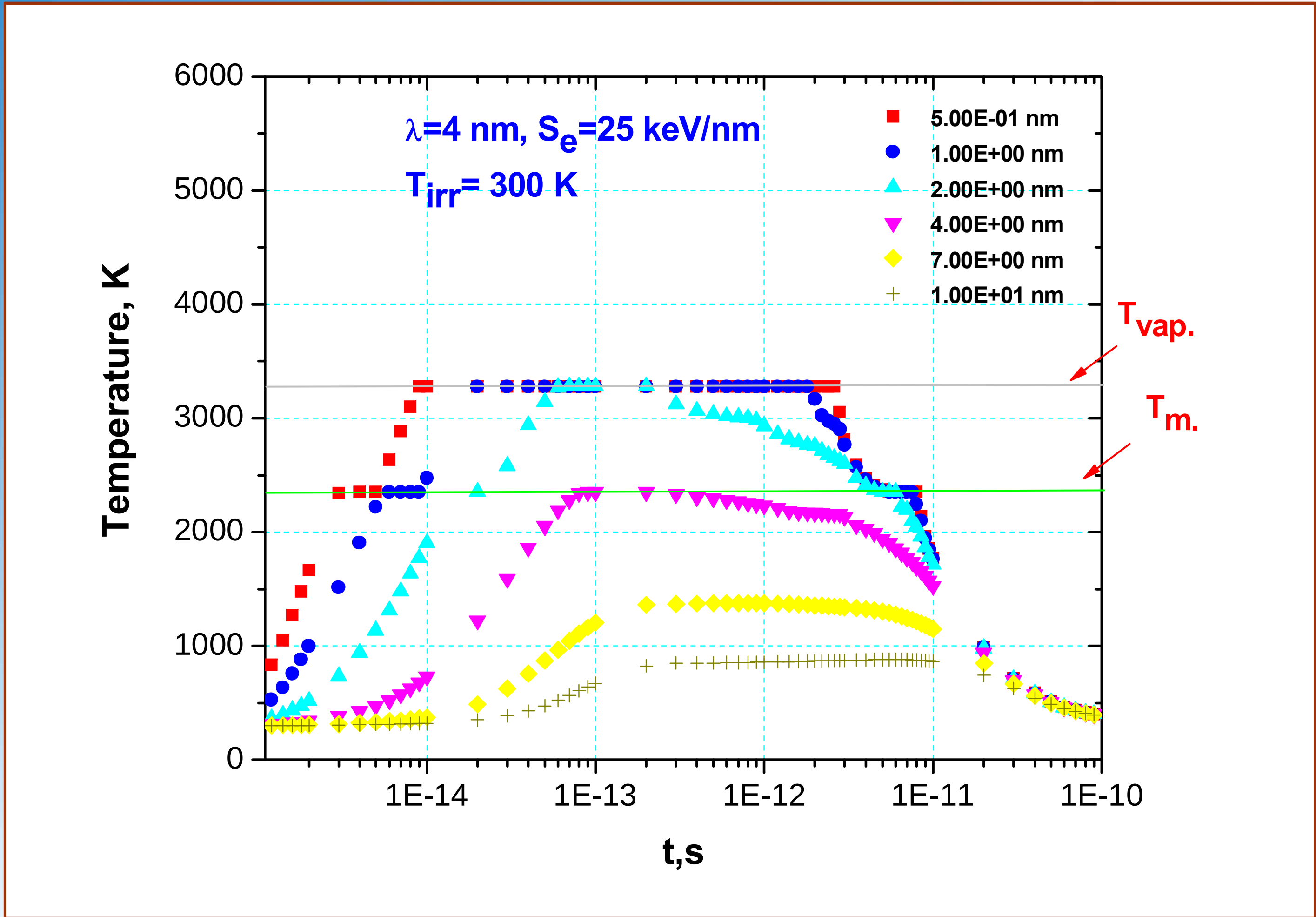

Temperature evolution at different radial distances from the Bi ion axis in sapphire. T_m = 2340 K, vaporization temperature is 3280 K. λ - electron-lattice interaction mean free path calculated with TSPIKE02 code. *M. Toulemonde, C. Dufour, A. Meftah, E. Paumier, Nucl. Instr. and Meth., B 166–167 (2000) 903*

Temperature dependent mechanisms of the hillock-like damage formation

2. An intense local heating followed by a rapid cooling stage leads to generation of thermoelastic stresses.

If R_c is effective track radius, the characteristic time of stress pulse is $\boldsymbol{2R_c/s}$, where $\boldsymbol{s}$ is the sound velocity. The radial tensile stress is defined as:

$$\boxed{\sigma_{rr} = \frac{\Gamma}{\pi^{1/2}}\rho\, cT_0\left[\alpha\left(\frac{r}{R_C},\frac{st}{R_C}\right) - \frac{1}{(1+\nu)}\frac{R_C}{r}\beta\left(\frac{r}{R_C},\frac{st}{R_C}\right)\right]}$$

Γ is Grüneisen parameter, ν - the Poisson ratio, ρ is the mass density, $\boldsymbol{c}$ -the specific heat and $\boldsymbol{T_0}$ – the peak temperature.

A.I.Kalinichenko and V.T.Lazurik, In "Radiation Acoustics", Ed. by L. M. Lyamshev. Nauka, Moscow, 1987, p. 27.

If R_c = 4 nm, T_0 = 3000 K, then radial tensile stress in Al_2O_3 will be ~ 20 GPa on track axis and about 2.5 GPa at r = 25 nm.

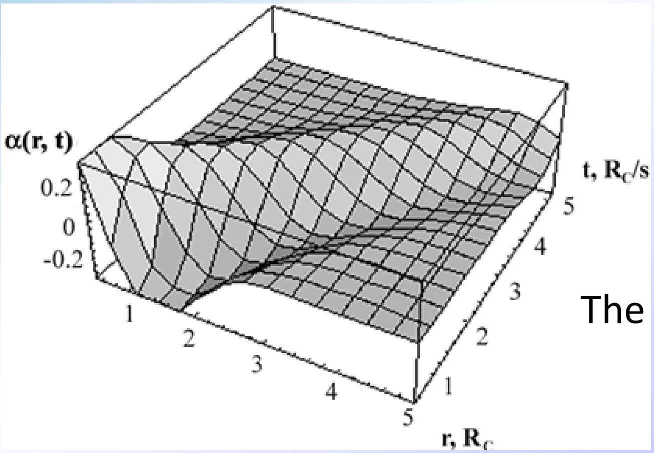

The radial component of the thermoelastic stress pulse at $r = 5R_C$

The basic feature of surface defects formation is local plastic deformation due to strain relaxation. The key questions are the nature of strain and the magnitude and dynamics of strain pulse in vicinity of the ion entrance point

Temperature dependent mechanisms of the hillock-like damage formation

Hillock formation from the ion-induced melt due to the mechanical stresses as a result of thermal expansion

G. Szenes,Nucl. Instr. Meth., B 191 (2002) 31

mean hillock height $h = gS_e+\beta S_n$

The necessary condition of hillocks production is the extension of the melt area:

$T_p > 2.7T_0$, $T_0 = T_m - T_{irr}$ $2.7T_0 = 5535$ K

If $T_p < 2.7T_0$, cooling starts with shrinking in spite of the presence of the melt and no hillocks should be formed

At S_e = 25 keV/nm Tp < 4500 K, while *2.7T0* = 5535 K. (TSPIKE02) .

Toulemonde, C. Dufour, A. Meftah, E. Paumier, Nucl. Instr. and Meth., B 166-167 (2000) 903.

Hillock formation as a result of the Coulomb explosion due to charge imbalance in the subsurface region

Quasineutrality of densely ionized region may be disturbed in the subsurface layer due to ejected electrons and incident ion charge neutralization process.

Baranov et al. Usp. Fiz. Nauk., 156 (1988), p. 477

Strong experimental indications for the occurrence of a macroscopic Coulomb explosion from a highly charged surface of crystalline Al_2O_3 under intense femtosecond laser pulse action have been reported recently

R. Stoian, D. Ashkenasi, A. Rosenfeld, and E. E. B. Campbell, Phys. Rev. B 62 (2000) 1367.

No surface profile modification have been detected under Kr^{+27} ion bombardment contrary to Bi^{+25} and Bi^{+17} ions. Ion charge neutralization cannot be the only condition for the hillock appearance

Summary (surface effects)

Mean hillock height on sapphire surface depends linearly on the incident electron stopping power and increases in two times on average when hillocks start to overlap.

Noticeable changes in defect shape are registered only under strong deviation from normal beam incidence (more than 60 degrees) and no specific features (radial coherent mass transport outwards from the track core) typical for shockwave-like mechanism were observed. The hock wave - like mechanism of the hillock formation could be ruled out of consideration

As a possible reason of hillocks formation, the plastic deformation due to the defects created by the Coulomb explosion mechanism in the target subsurface layer is suggested

Elaboration of atomostic mechanisms responsible for the hillocks production requires the use of MD simulation methods

The modification of the thick NC- SiO_2 layers with random NC distribution by high energy ion irradiation.

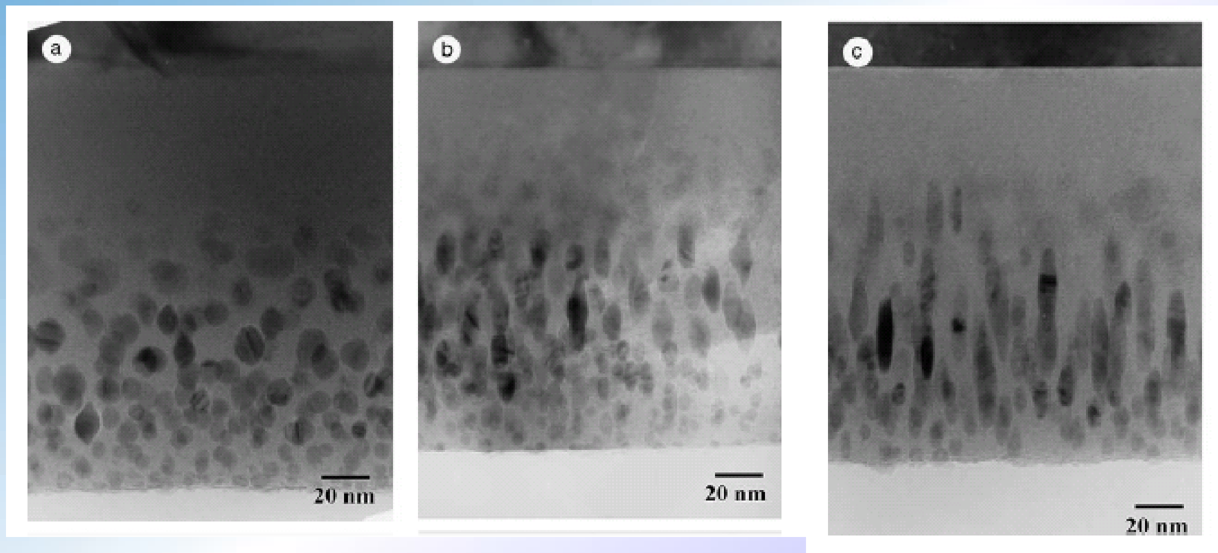

Co NC in SiO_2 before (a) and after irradiation by 200 MeV I with doses ~10^{12} (b) and ~10^{13} cm^{-2} (c). [C.D'Orleans, NIM B, 216, 2004, 372, Phys. Rew. B, 67, 2003, 220101]

SiO_2 layers with variable NCs concentration

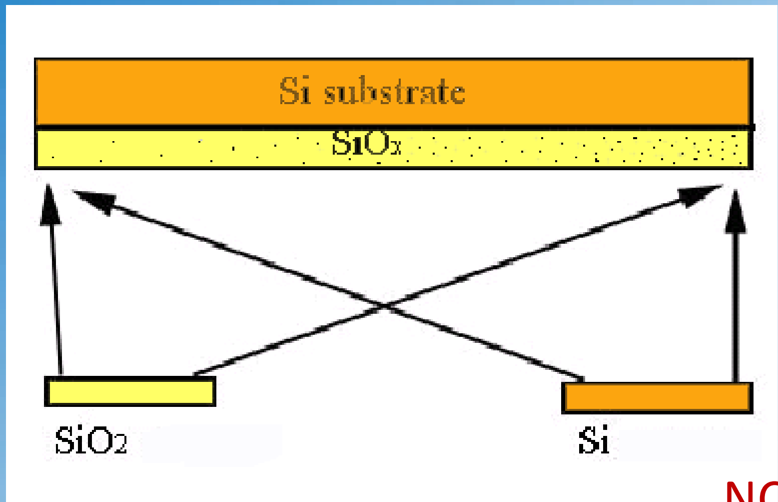

1. Deposition of SiO_2 and Si on Si substrate from two sources separated by distance of 100 mm
2. d_{SiO2} = 400 - 1000 nm
3. Si content in oxide: 4 - 94 vol.%
4. Annealing: 1140^{o}C, 40 min, N_2

NC size: 3 – 5 nm

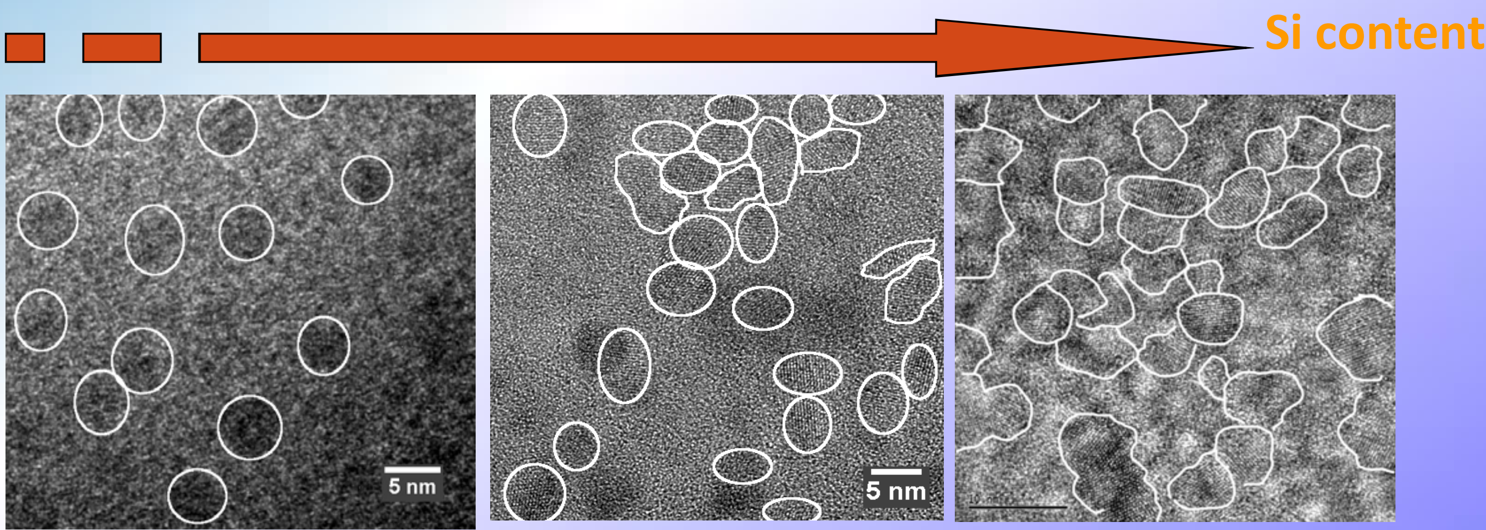

NC concentration increased with coordinate along the sample

Modification of the NCs

		Se	Ion fluence
Kr, 90 MeV,	R_p = 16 mm	7.1 keV/nm	
Xe, 130 MeV,	R_p = 17 mm	10.2 keV/nm	10^{12}-10^{13} cm^{-2}
Bi, 670 MeV,	R_p = 43 mm	18 keV/nm	

TSPIKE-02

M.Toulemonde , 2000

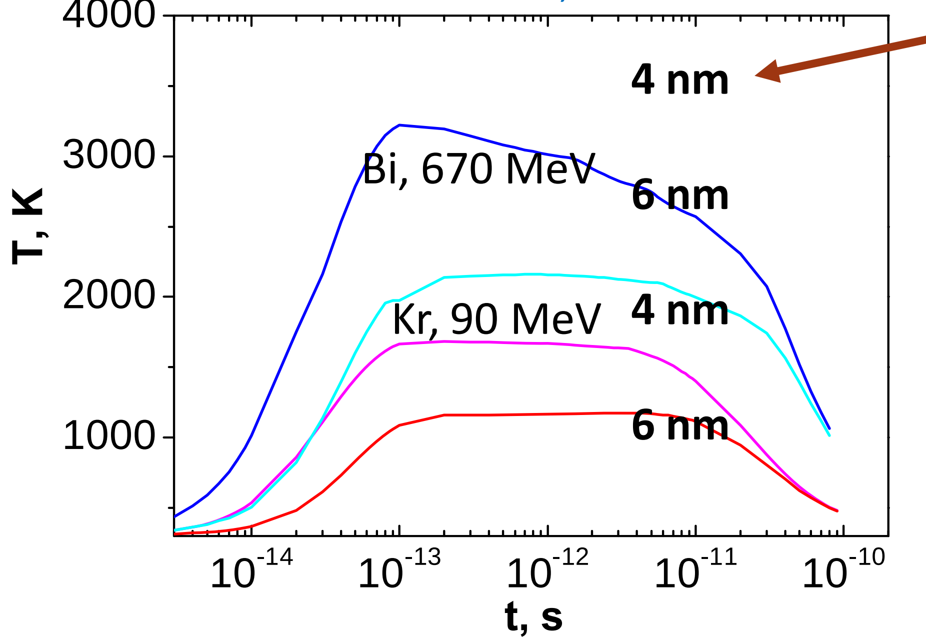

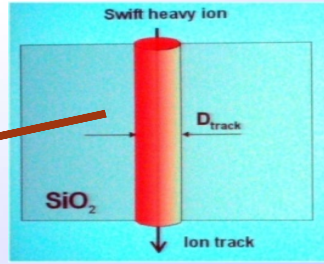

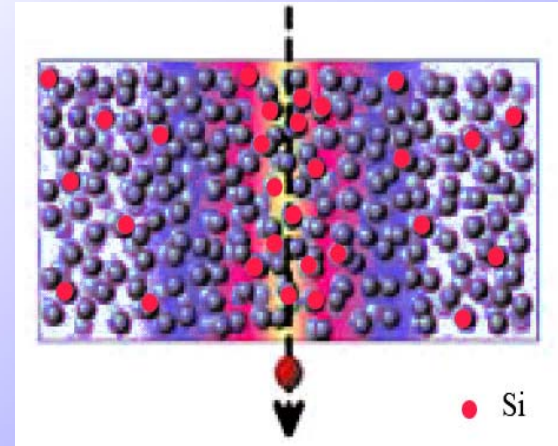

Modification of the NCs

Irradiated NC-SiO_2 layer
(37% Si) Kr, 90 MeV, 10^{12} cm^{-2}

surface

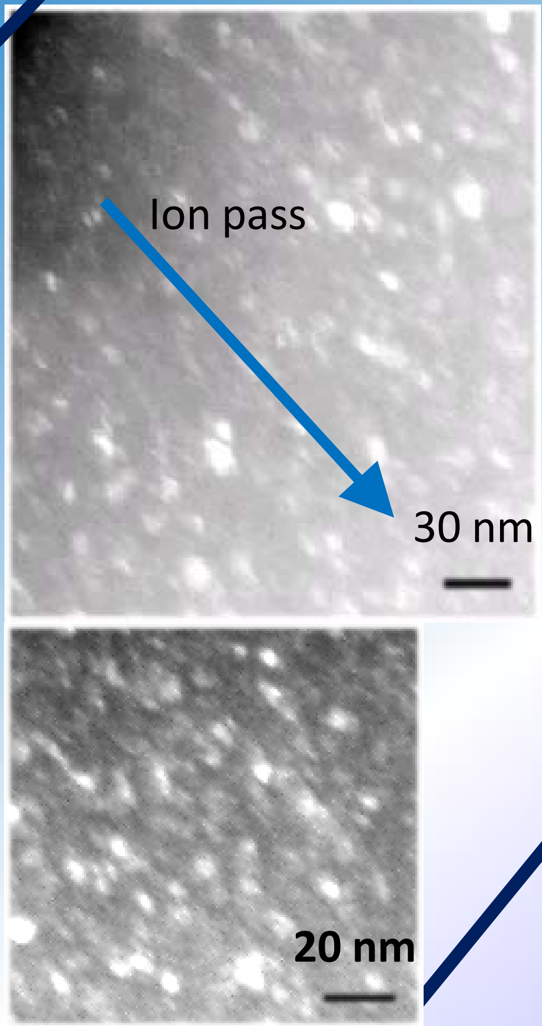

substrate

Raman spectra

Ar, 514 nm

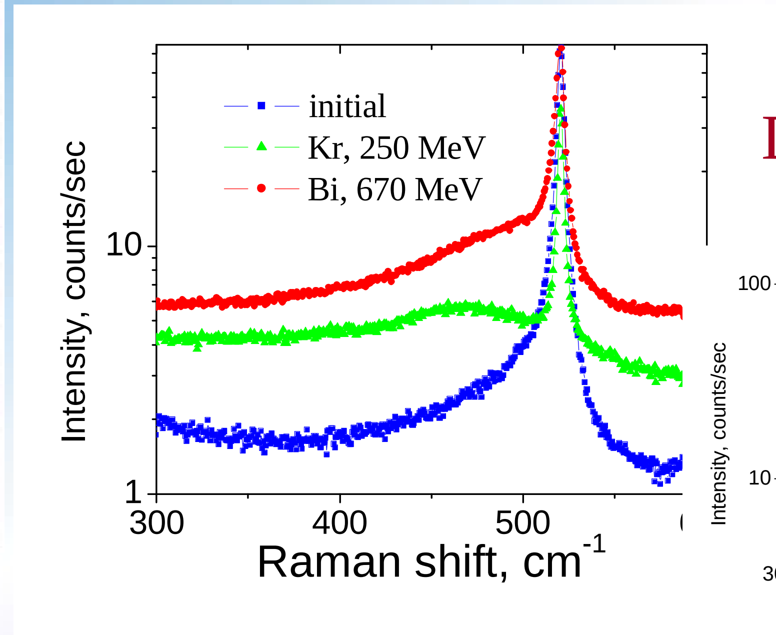

Differential spectrum

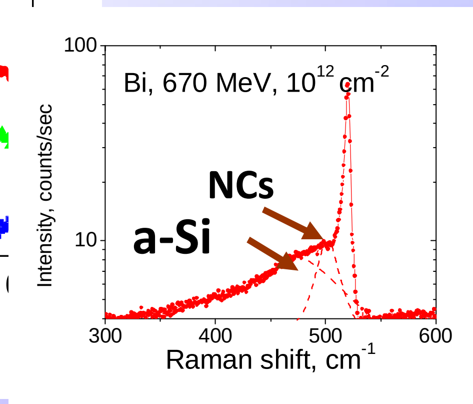

Formation of new NCs becomes more pronounced with increase in ion energy. Increase in the ion dose and decrease in ion energy lead to appearance of the amorphous Si inclusions.

Formation of the new NCs and the ordered NC distribution

I.V. Antonova, Nanotecnology, 2009

Modification of the NCs

HREM cross sectional images for the Si NCs in irradiated layer

Kr, 90 MeV, 10^{12} cm^{-2}

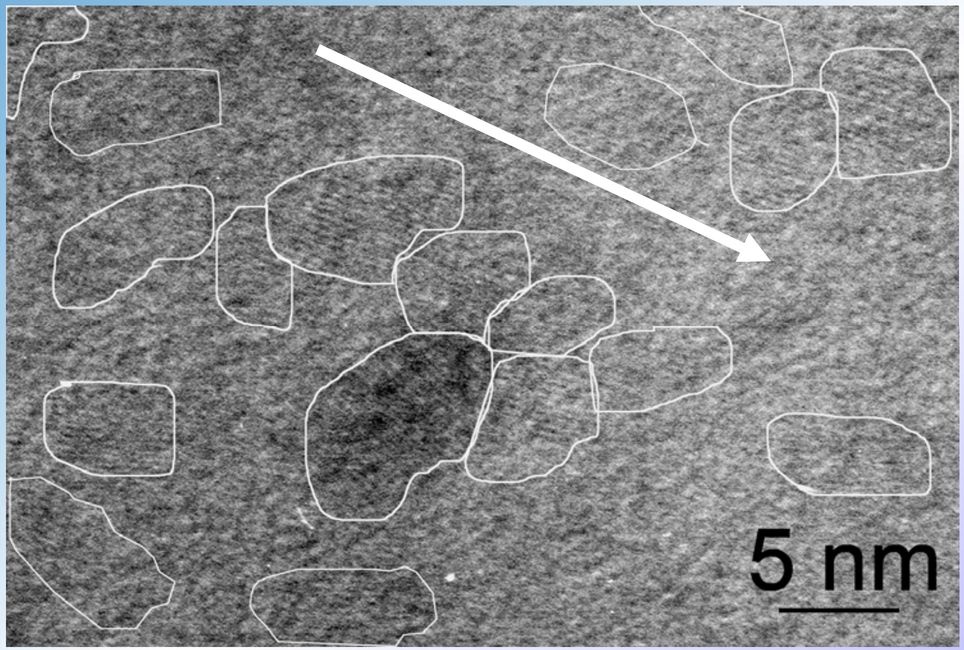

non-irradiated layer

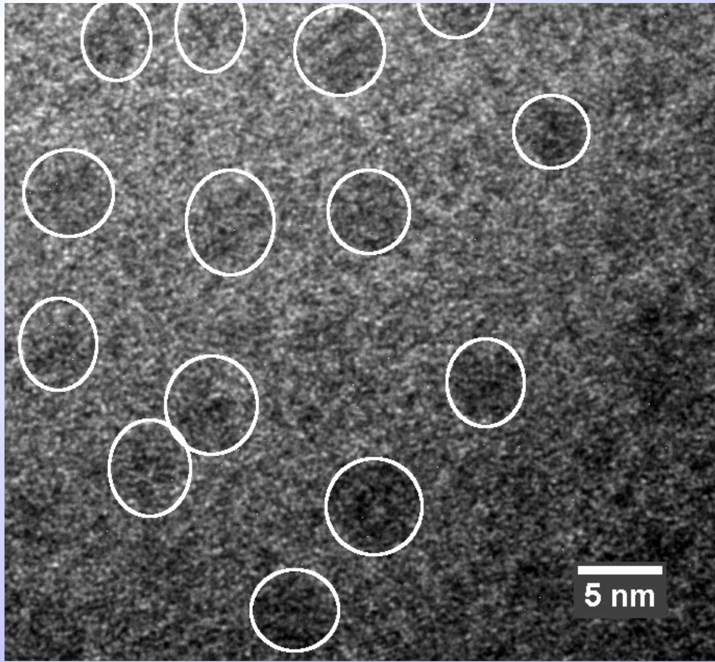

Atomic planes of NCs in the irradiated samples are oriented along ion tracks

Percolation conductivity

Bi, 670 MeV

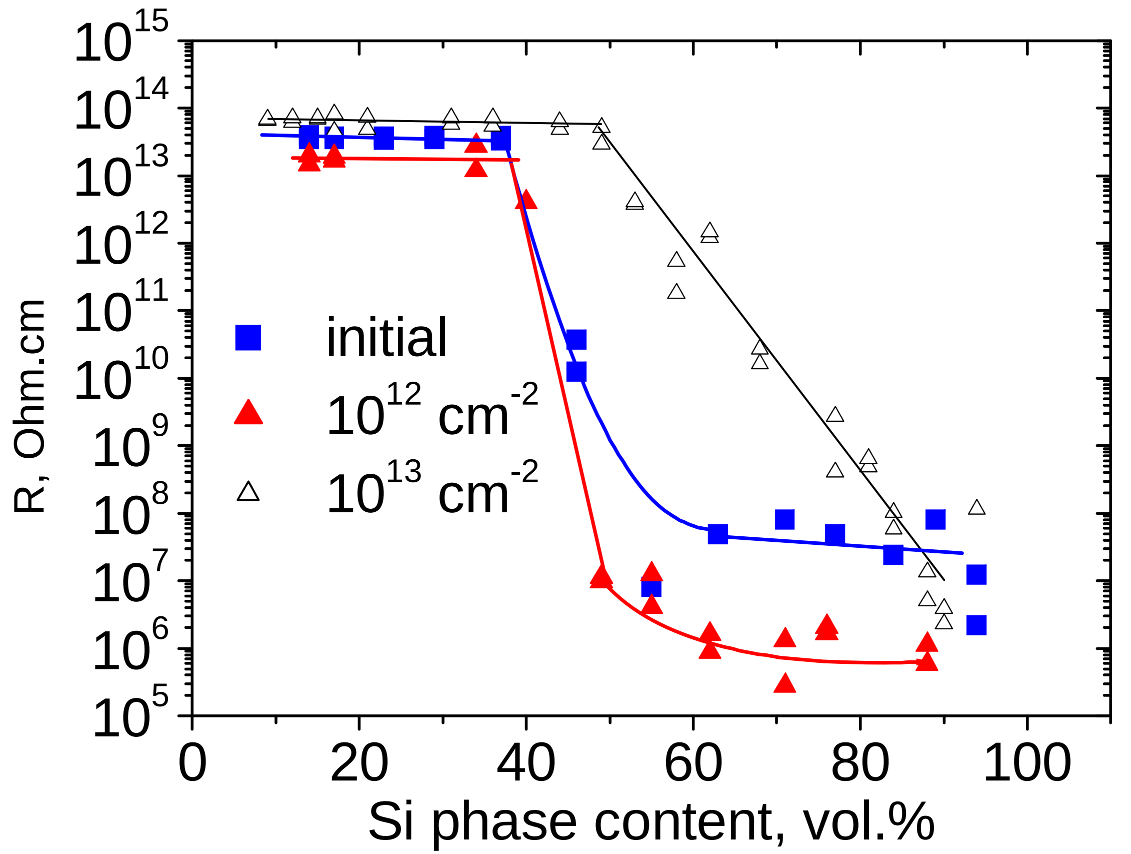

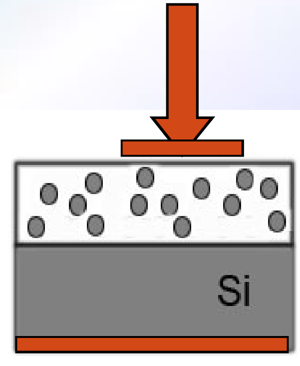

I.V. Antonova et al, Solid State Phenomena 156 – 158, 523 (2010).

Conductivity of irradiated NC-SiO_2 layer is increased after irradiation with low ion fluences

Resonant tunneling effect

Kr, 90 MeV, 10^{12} cm^{-2}

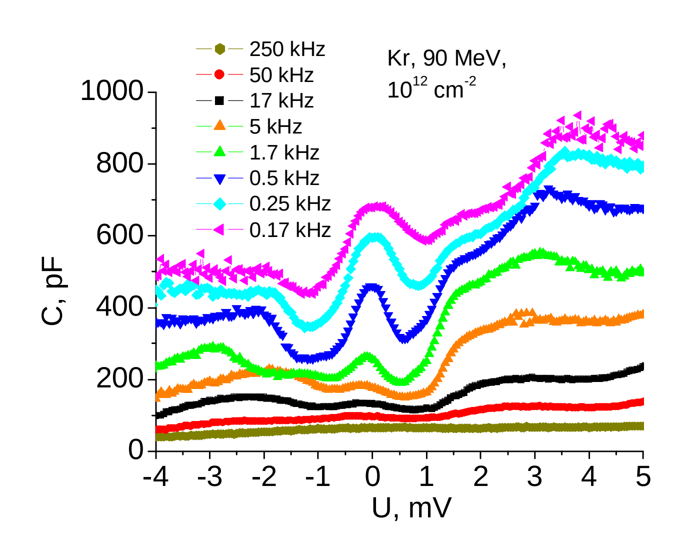

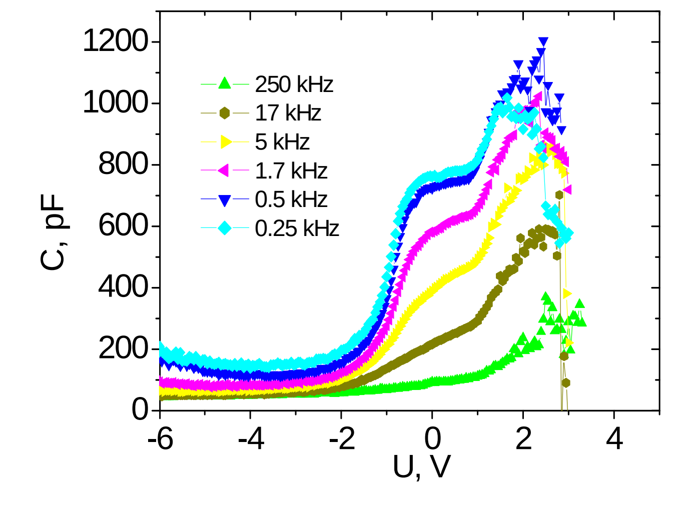

Pristine non-irradiated sample

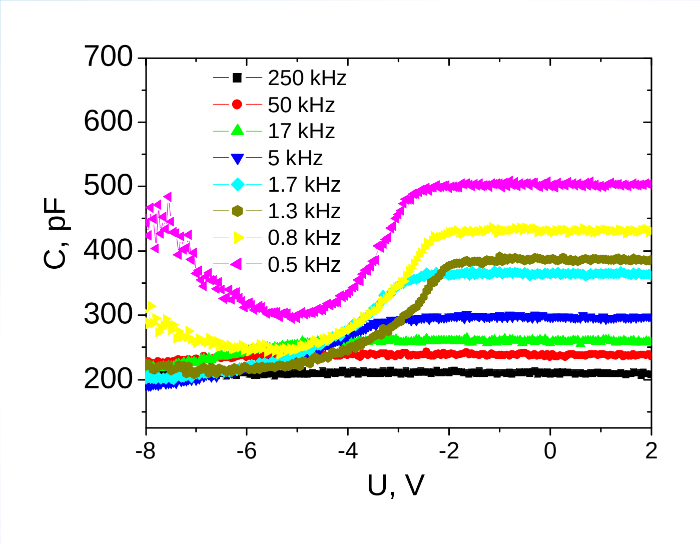

I.V.Antonova et al, Nanotechnology, 20, 185401 2009

Capacitance peaks are found in C-V characteristics for Si content > 50% in ion beam treated samples.

Resonant tunneling effect

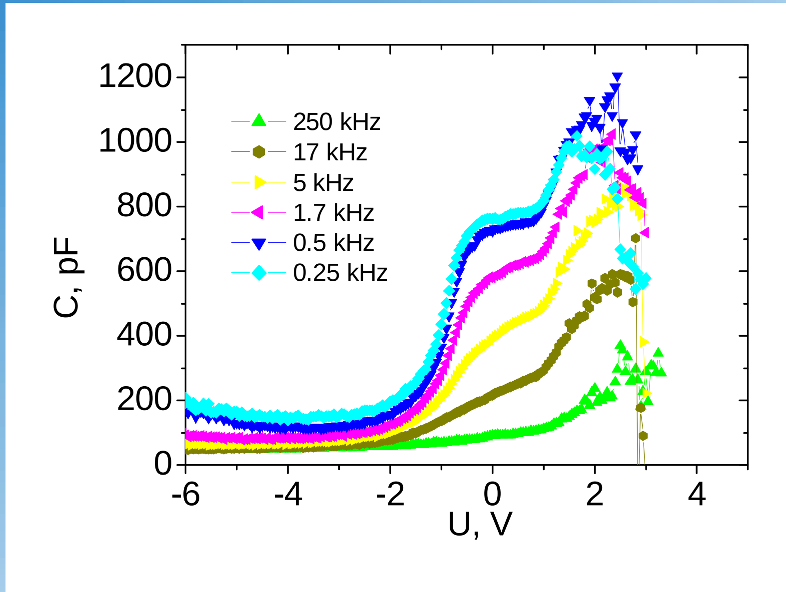

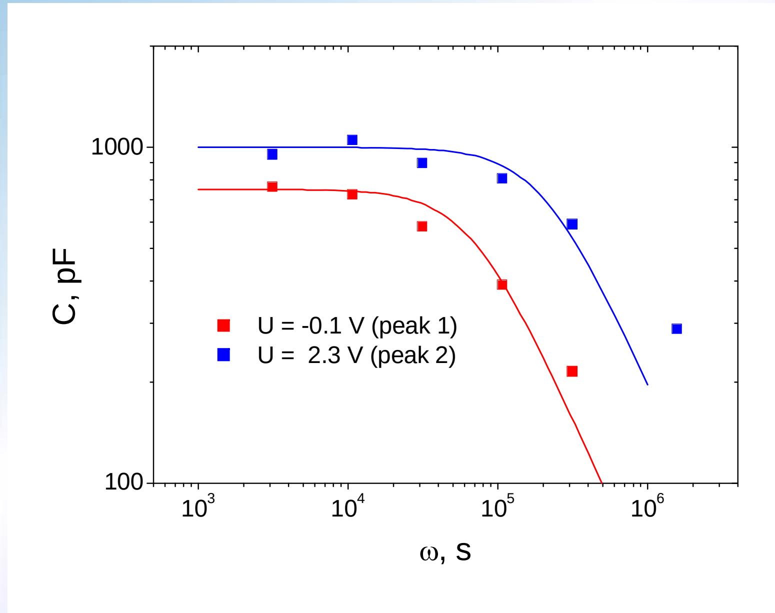

$$C(\omega) = \frac{C_{\max}}{\sqrt{(1+(\omega\tau)^2}}$$

$$t \sim T^{-1} \quad T = \exp\left(-\frac{2}{\hbar}\int_{x_2}^{x_1} p\,dx\right) \sim \exp\left(-\frac{d}{\lambda}\right), \quad \lambda = \frac{h}{\sqrt{2mE}}$$

Peak 1 (-0.1V) $\tau_1 = 1.5\text{x}10^{-5}$ s

Peak 2 (2.3V) $\tau_2 = 5\text{x}10^{-6}$ s

$$\ln\left(\frac{\tau_2}{\tau_1}\right) = \frac{h}{d\sqrt{2m}}\left(E_1^{-1/2} - E_2^{-1/2}\right)$$

NC size estimated from τ_1 and τ_2 values is equal to 3.3 nm which correlated with PL and TEM data

Resonant tunneling effect

Bi, 670 MeV, 10^{12} cm^{-2}

$\Delta E_e = e/C_{nc} = kx0.5$ V

$\Delta E = keDV = k\,x2.6V$

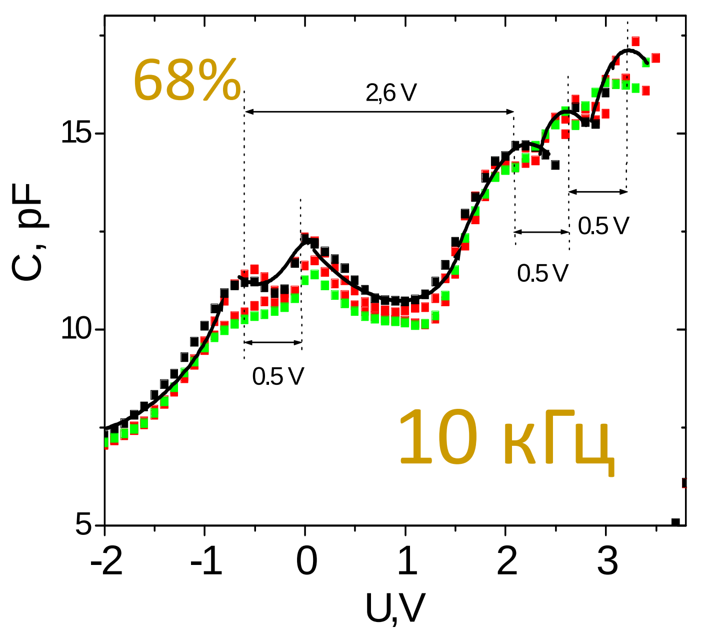

I.V.Antonova et al, Nanotechnology, 20, 185401 2009

NCs size W = 3.3 nm

$\Delta E = E_2 - E_1 \sim 100$ meV

k = 0.048

$\Delta E_c = e/C_{nc}$

$\boldsymbol{\Delta E_c = 24}$ **meV**

$C = 8x10^{-18}$ F

Charging energy of QDs was estimated as $\Delta E_e = 24$meV and the capacitance of the QDs was estimated as 8 aF

Resonant tunneling effect

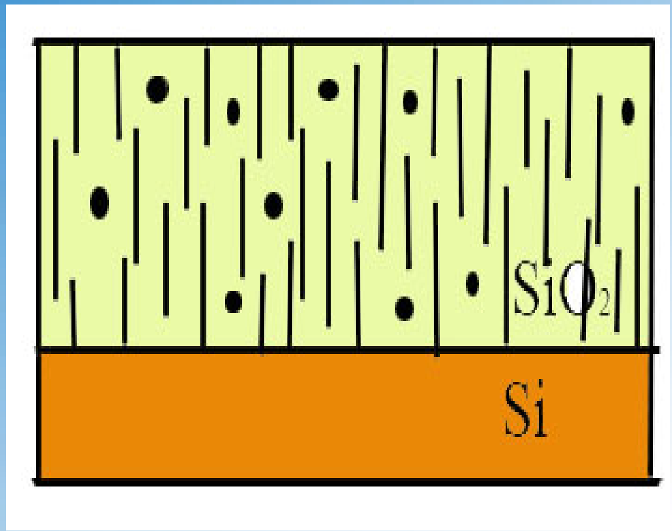

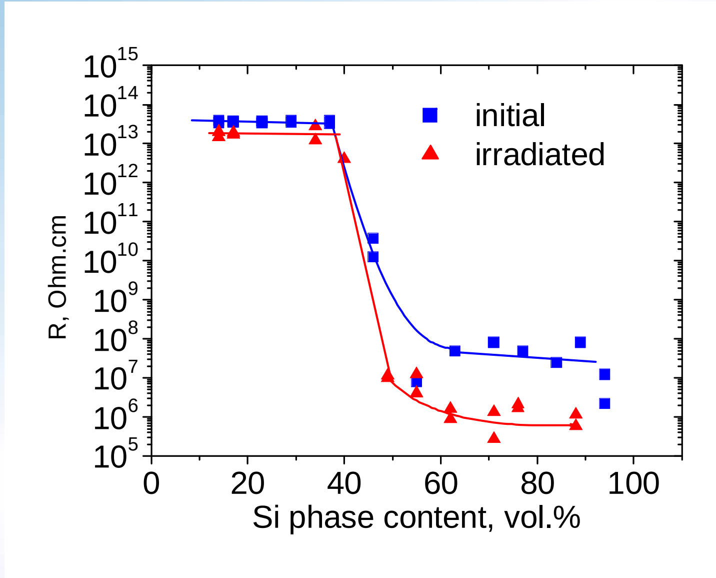

C-peaks are explained as resonance tunneling of carriers to NCs due to formation of the conductive network, which play the role of conductive substrate for two-dimensional arrays of QDs located in cells outside the net.

Density of NCs give a contribution to C-peak formation was estimated as 10^9 cm^{-2} (whole NC density ~ $2\text{x}10^{12}$ cm^{-2})

Photoluminescence of NCs

Xe, 130 MeV, 10^{12} cm^{-2}

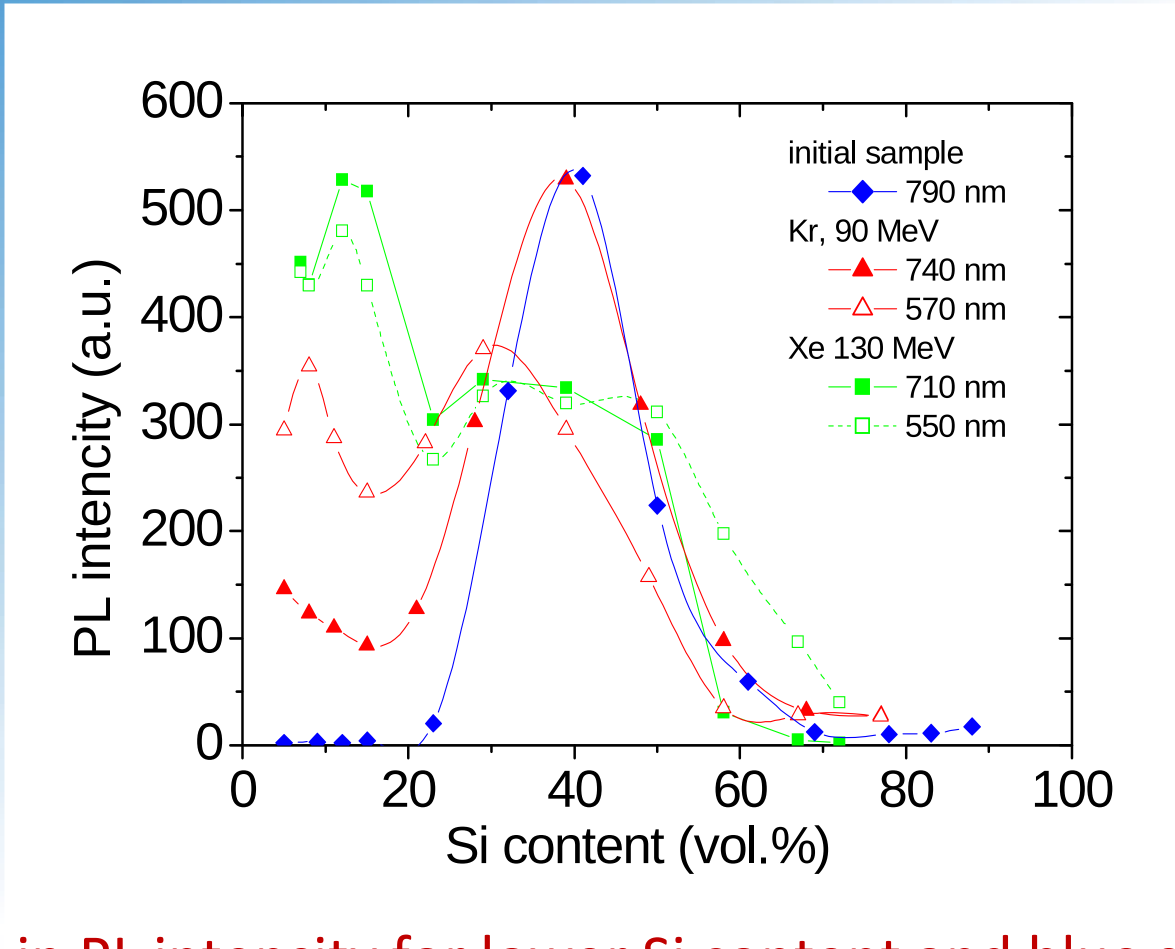

Increase in PL intensity for lower Si content and blue shift of PL peak in spectrum due to decrease in NC size

SiO_2 layers with variable Ge-NCs concentration

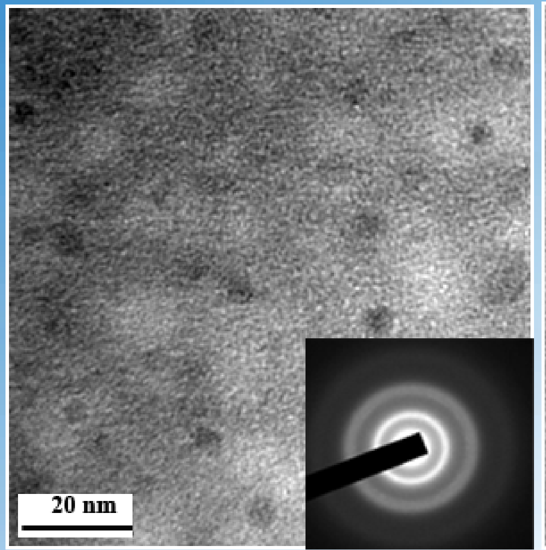

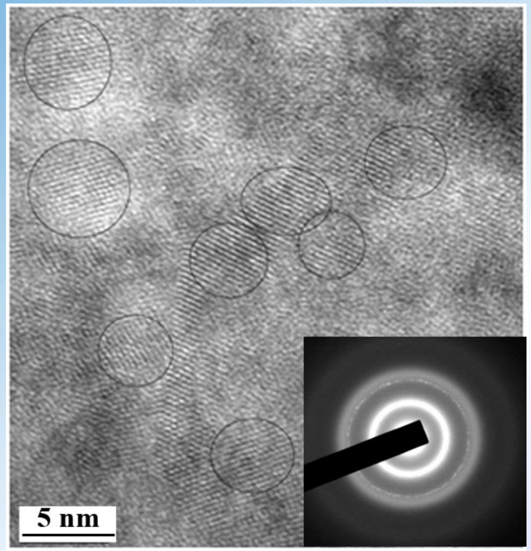

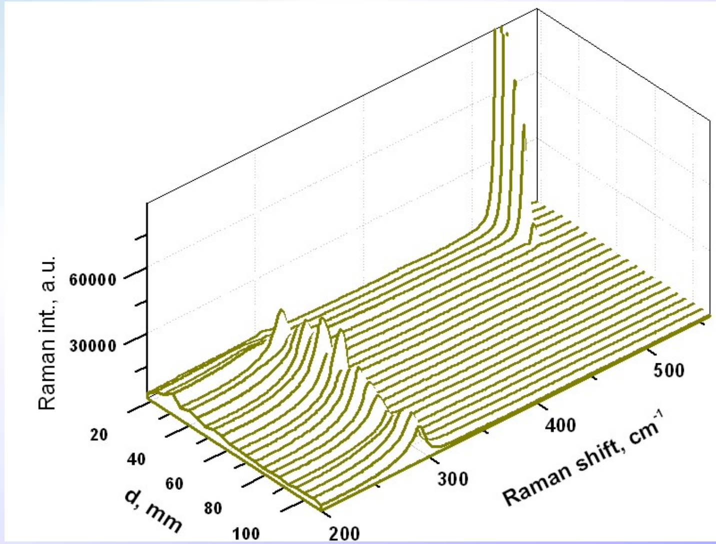

NCs with a size of 2–5 nm were revealed in layers of irradiated and subsequently annealed (at 500°C) films. Without irradiation, only amorphous Ge inclusions were observed in layers annealed under the same conditions

*I.V. Antonova et al. J. Phys. D: Appl. Phys. **45** (2012) 285302*

Summary (NCs)

Swift heavy ion irradiation was found to lead to following functionalization of the silicon nanocrystals in SiO_2 matrix:

Formation of the ordered NC distribution along the ion tracks through the 400-1000 nm layer, yielding NC chains, or a global conductive NC network with the increase in the Si phase content.
Utilization of the ion fluences ($\geq 10^{12}$ cm^{-2}) leads to decrease in NC size (or diameter of aligned NCs).
Barrier energy for the carrier emission from isolated NCs in modified NCs-SiO_2 layers and the low temperature emission times decrease after ion beam treatment.
Functionalization is also included such attractive effects as formation of new NCs under irradiation, increase in PL intensity, appearance of additional quantum effects for irradiated layer and other.

Radiation stability of nanocrystalline ZrN against fission fragments impact

ZrN exhibits excellent radiation resistance against low-energy heavy ion bombardment

G.W. Egeland et al. Heavy Ion Irradiation Effects in Zirconium Nitride. In: Proceedings of the 2004 International Congress on Advances in Nuclear Power Plants, ICAPP'04, vol. 4225, 2004, 2023.

Material	S_{et}, keV/nm	Ref.
AlN	**> 34**	S.J. Zinkle, J.W. Jones, V.A. Skuratov. MRS Symposium Proceedings, Vol. 650, MR, Warrendale, PA, 2001, p. R3.19.1. S.J.Zinkle, V.A.Skuratov and D.T.Hoelzer. NIMB 191(2002) 758
	> 21.6	S. Mansouri et al. // NIMB 266(2008) 2814
BN	**> 17.6**	S. Mansouri et al. // NIMB 266(2008) 2814
SiC	**>34**	S.J. Zinkle, J.W. Jones, V.A. Skuratov. MRS Symposium Proceedings, Vol. 650, MR, Warrendale, PA, 2001, p. R3.19.1.
SiC **Nano-SiC**	**> 22** **> 17**	A. Audren et al. // NIMB 267(2009) 976, NIMB 266 (2008) 2806
Nano-ZrN	**> 49**	A. Janse van Vuuren, V. A. Skuratov, V.V. Uglov (in press)
Si_3N_4	**15**	S.J. Zinkle, J.W. Jones, V.A. Skuratov. MRS Symposium Proceedings, Vol. 650, MR, Warrendale, PA, 2001, p. R3.19.1. S.J.Zinkle, V.A.Skuratov and D.T.Hoelzer. NIMB 191(2002) 758

Nitride and carbide based ceramics have a low sensitivity to electronic stopping power effect

Formation of nitride coatings

Equipment for deposition (VU-2MBS)

ZrN coatings were formed by Cathodic Arc Vapor Deposition (CAVD) technique.

Pretreatment: $p = 10^{-3}$ Pa, U_{bias}= -1 kV, I_{Zr}= 100 A.

Deposition parameters: $p_N = 10^{-1}$ Pa, U_{bias}= – 120 V, I_{Zr}= 100 A.

deposition time 15-18 s, 10-11 min, 40 min.

Objects: CAVD coatings ZrN / Si , ZrN/SS

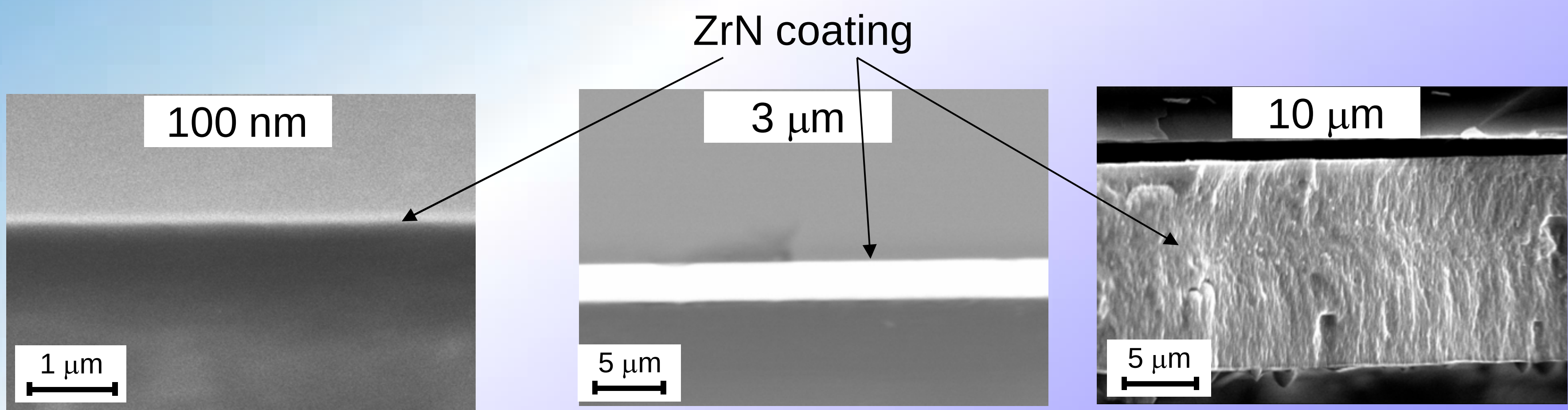

Radiation stability of nanocrystalline ZrN against swift heavy ion irradiation

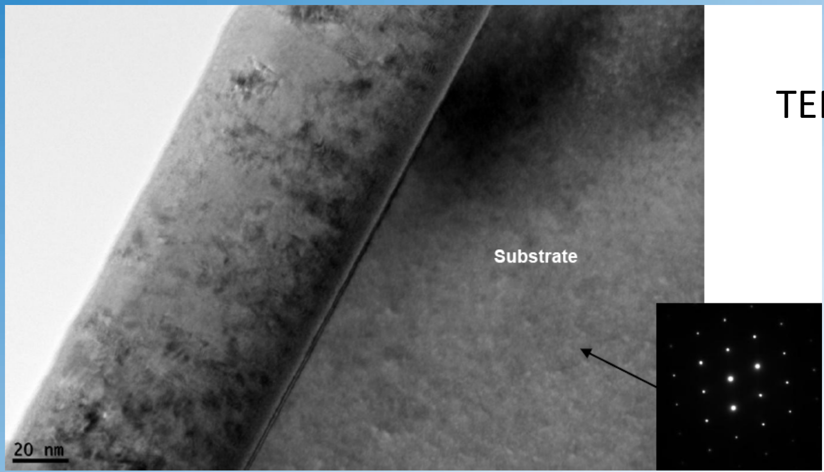

TEM image of as-grown 80 nm ZrN layer

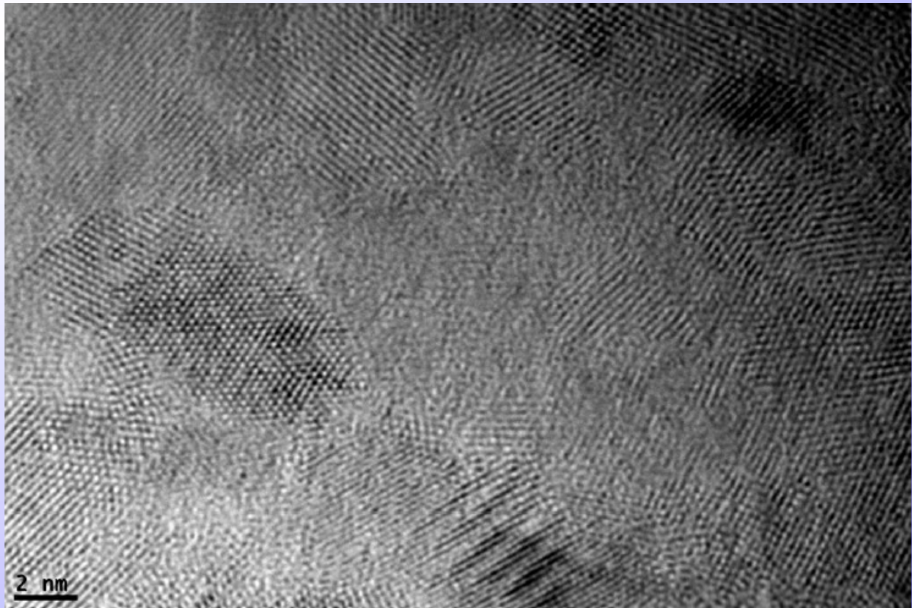

Bright field TEM micrograph of virgin ZrN sample

Radiation stability of nanocrystalline ZrN against swift heavy ion irradiation

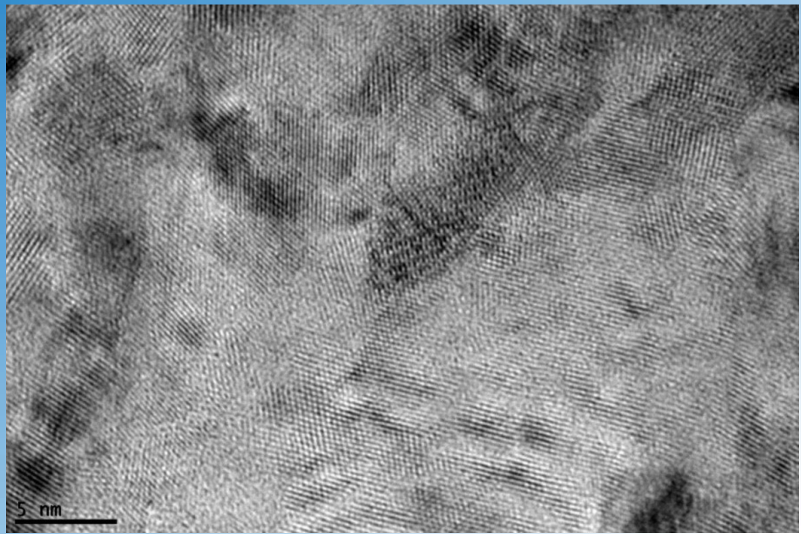

Bright field TEM micrograph of 167 MeV Xe irradiated ZrN sample (ion fluence 1.3×10^{15} cm^{-2})

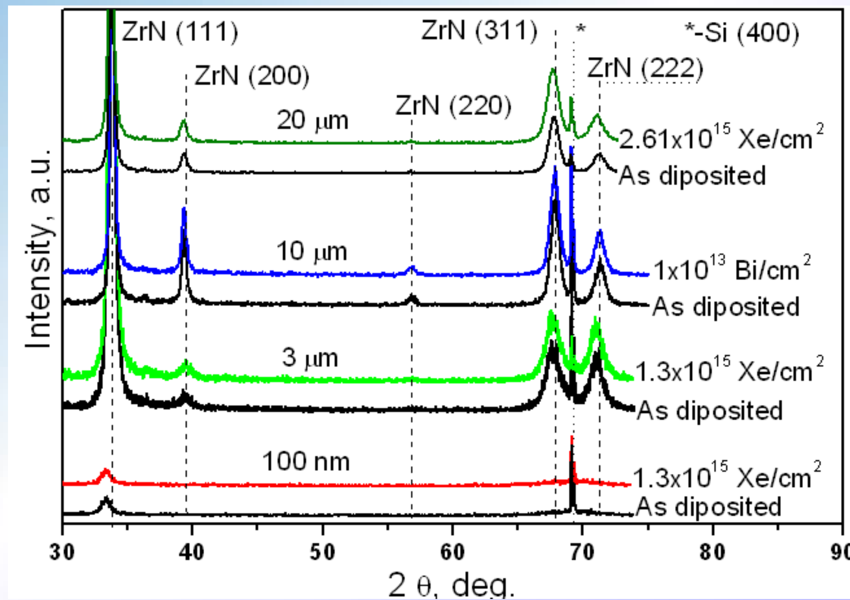

X-ray diffraction spectra of virgin and ion irradiated (167 MeV Xe and 695 MeV Bi) zirconium nitrides layers grown on Si substrate

- The phase composition of nanocrystalline ZrN is not changed after heavy ion irradiation at electronic stopping power up to 49 keV/nm
- TEM examination does not reveal latent tracks formation in ZrN irradiated with heavy ions of fission fragments energy

Oxide nanoparticles in the ODS alloys irradiated with swift heavy ions

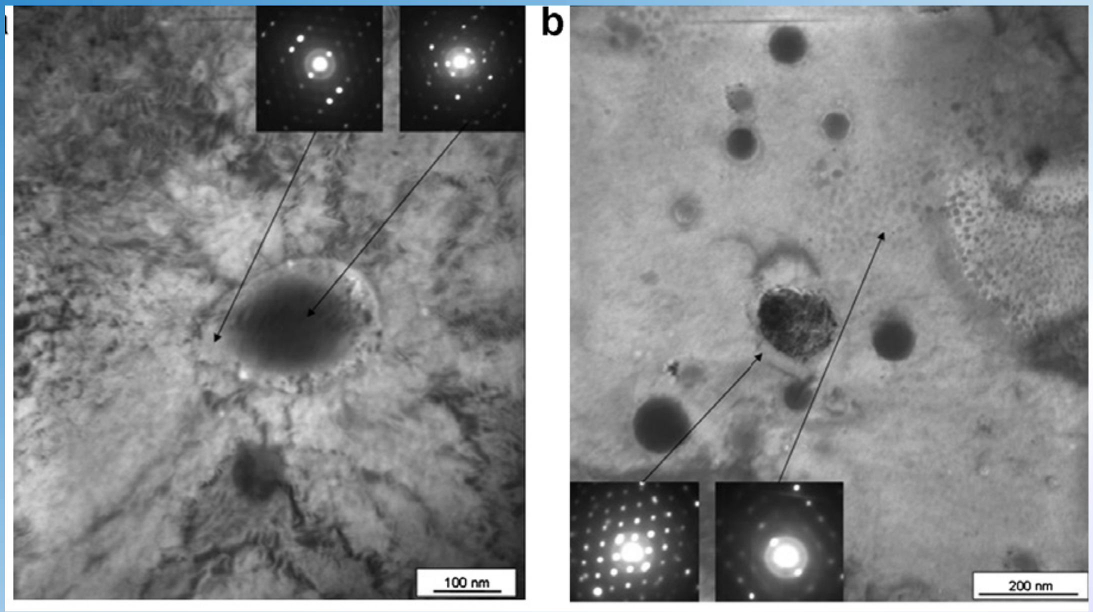

Dispersion and crystallinity of the oxides in DY (Fe–13Cr–1.5Mo) ODS alloy after 92 MeV Xe ion irradiations at RT

Ribis et al., JNM 417 (2011) 262-265.

Electronic excitations may induce phase transition to amorphous state in ODS alloys. These amorphous precipitates are coexisting with other precipitates which remain crystalline

First results on high-energy heavy ion irradiation of the ODS steels

M.-L. Lescoat et al., J. Nucl. Mater. 417 (2011) 266-269.
Ribis et al., J. Nucl. Mater. 417 (2011) 262-265.
I. Monnet et al., J. Nucl. Mater. 424 (2012) 12–16.

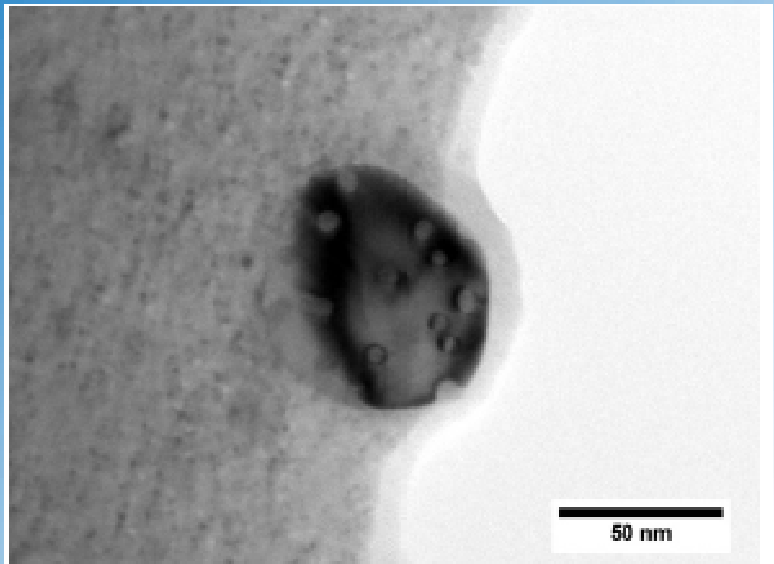

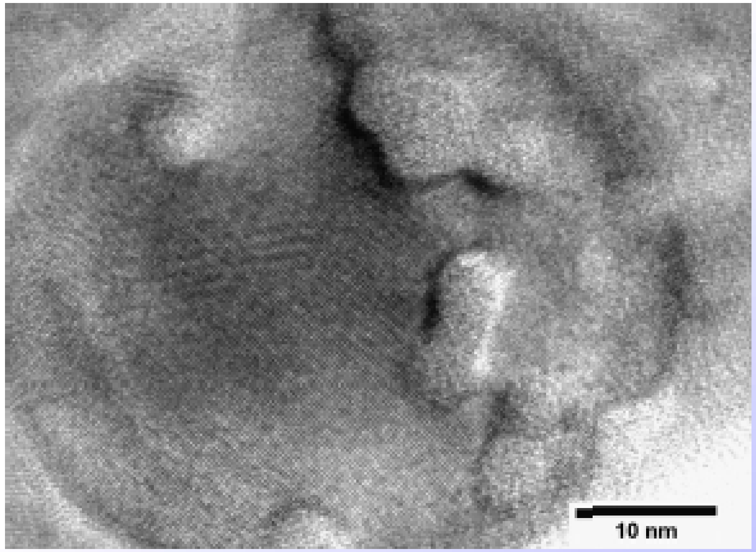

Conventional TEM image of round spots in a large oxide of the DY ODS alloy after 74 MeV Kr ion irradiation at 10^{12} cm^{-2}

HRTEM image of amorphous tracks in a crystalline oxide of the DY ODS alloy after 74 MeV Kr ion irradiation at 10^{12} cm^{-2}

I. Monnet et al., J. Nucl. Mater. 424 (2012) 12–16.

Materials:

1. KP-4: Fe-15Cr-4Al-2W-0.35Y2O3 (Kyoto University)

wt	Cr	Al	Zr	Y	O	N	Ar
KP-4(-3)	15.4	3.8	0.32	0.26	0.17	0.011	0.005

2. Cr16 (VNIINM, Moscow)

Elements	Fe	Cr	W	Ni	Mo	Y
Elements ratio, wt. %	83,1	16	2,0	<0,1	<0.1	<0,1

Ion irradiation parameters

Xe (167 MeV, $1\times10^{14} \div 2.56\times10^{15}$ cm^{-2}) Bi (700 MeV, $1.5\times10^{12} \div 1.5\times10^{13}$ cm^{-2}) $T_{irr.}$: 300K

Experimental techniques: TEM, SEM, EDX, XRD

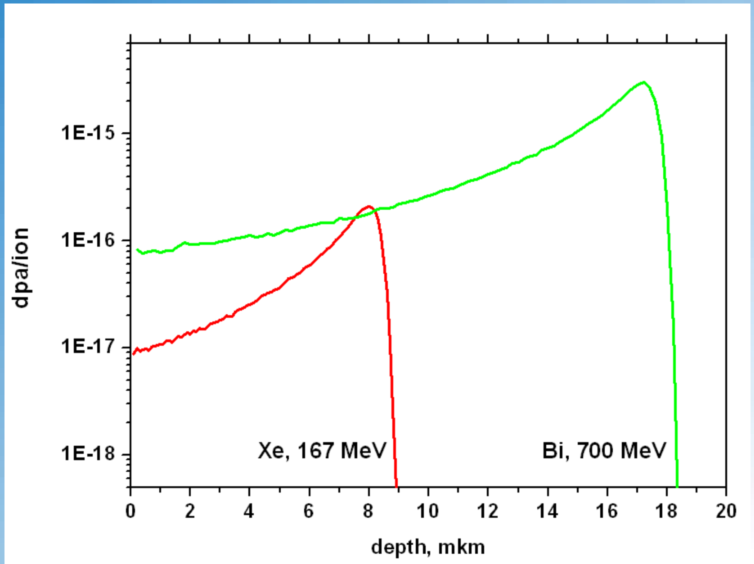

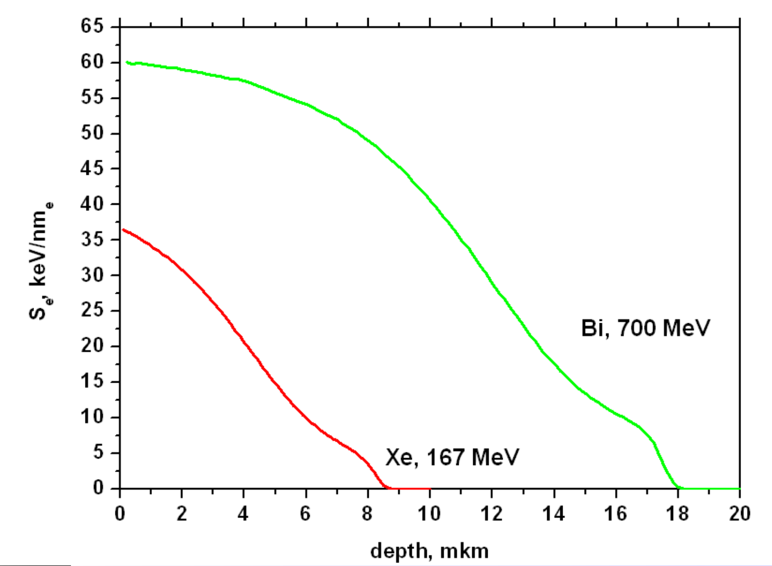

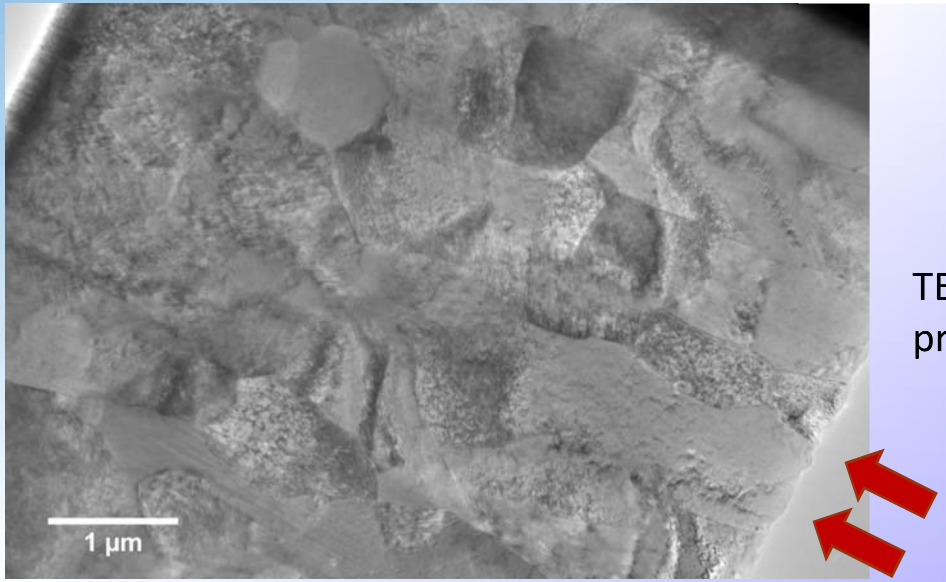

TEM micrograph of the FIB prepared target (KP-4)

Ion beam direction

KP4 as-received

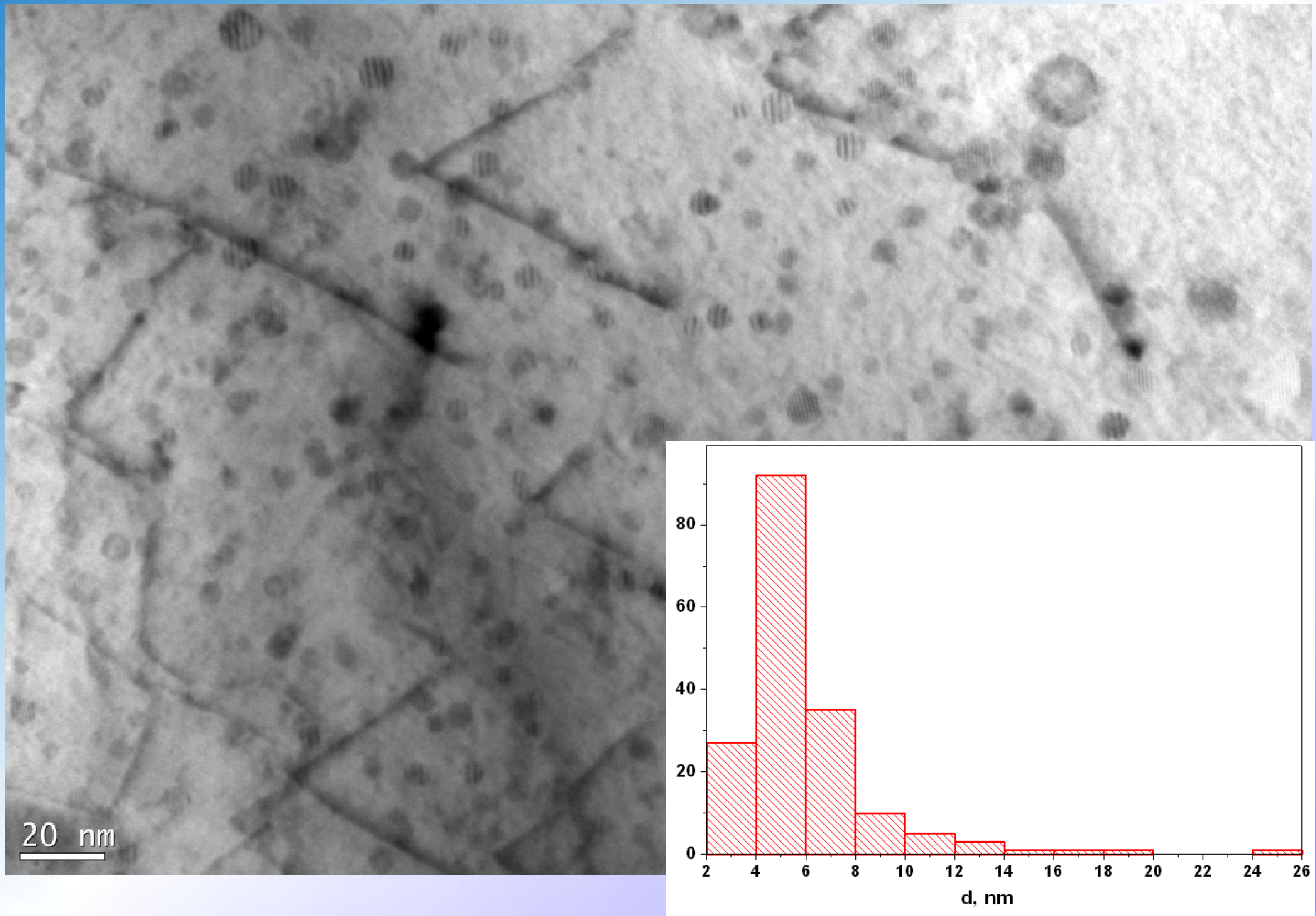

Oxide size distribution in the non-irradiated material

Oxide nanoparticle inKP4 steel (as-received)

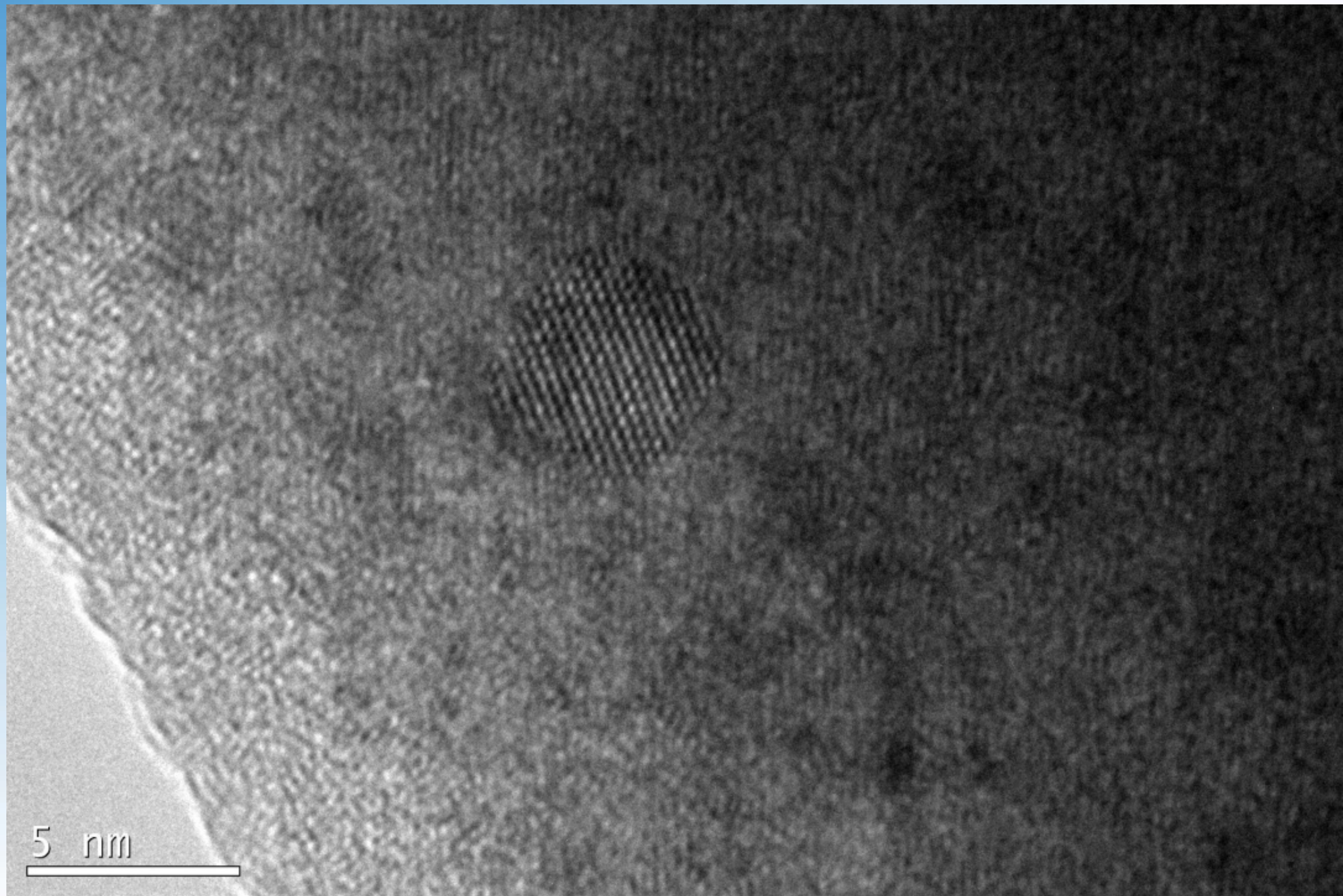

Cr16 as-received

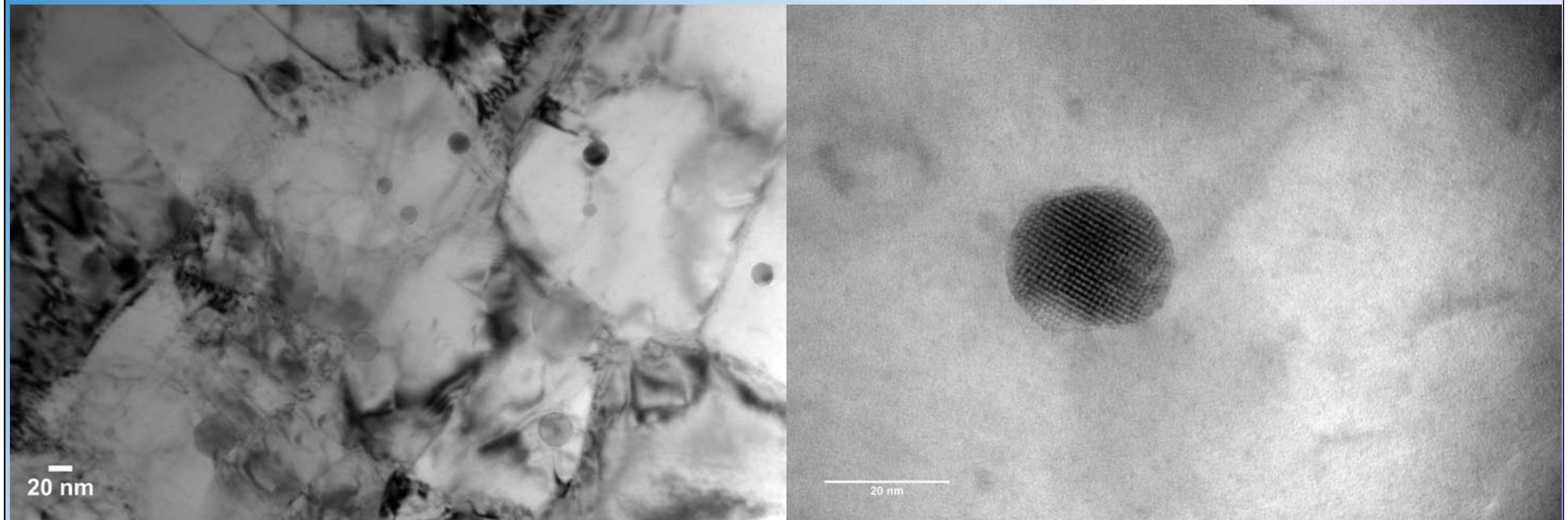

Cr16 + Bi 1.5e13 cm^{-2}

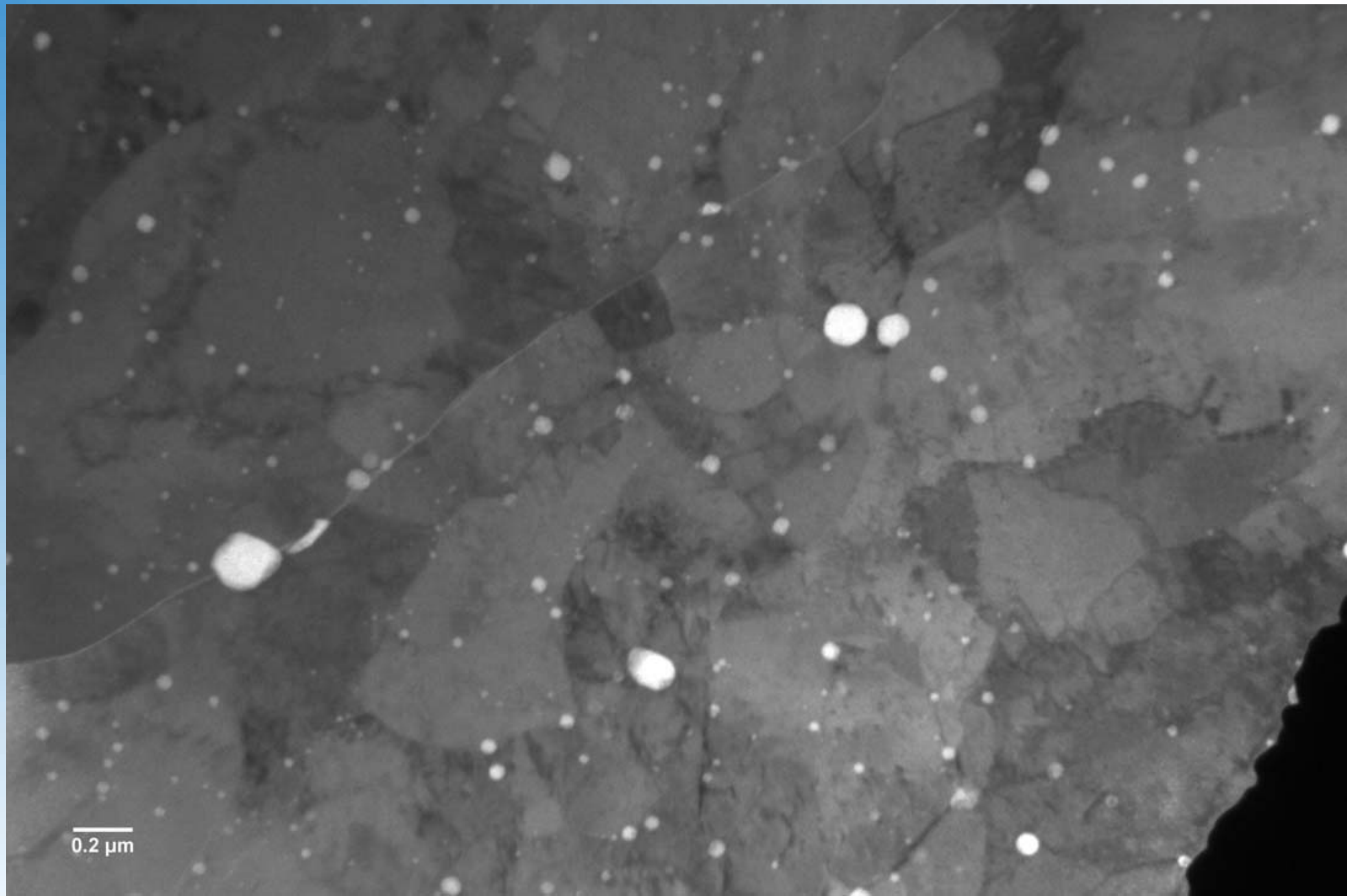

Cr16+ Bi, 1.5e13 cm^{-2}

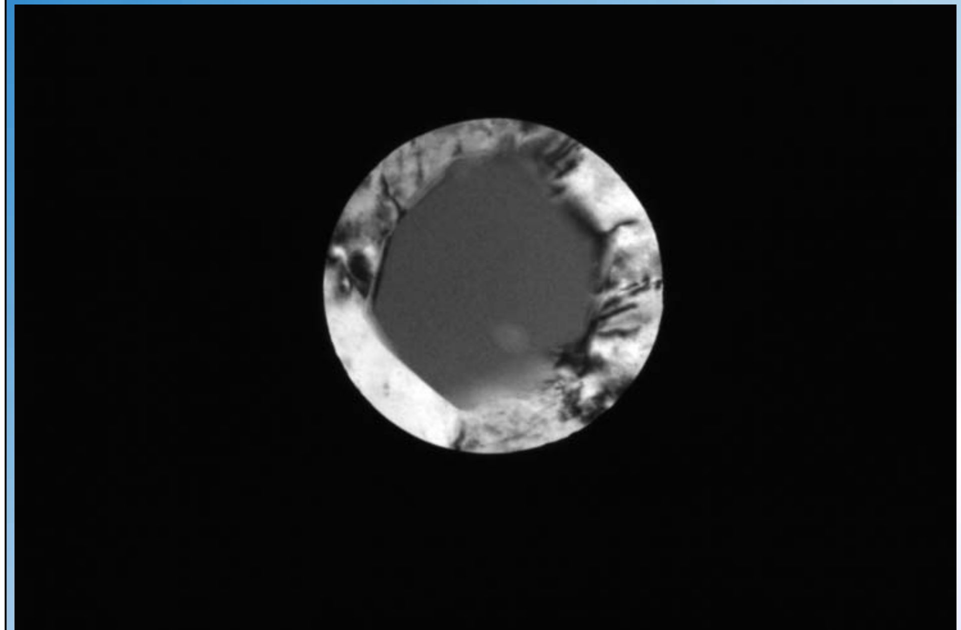

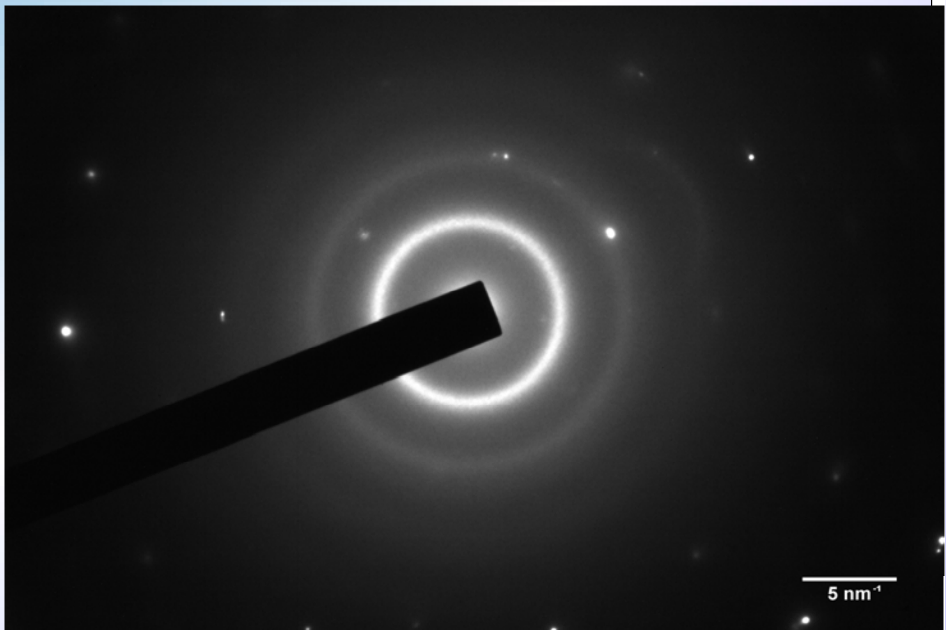

Irradiation of the Cr16 ODS steel by 167 MeV Xe and 700 MeV Bi ions in the ion track overlapping regime leads to complete amorphization of Y_2O_3 particles

Phase composition

Cr16 + Xe (167 MeV, $2.78 \cdot 10^{14} \div 2.56 \cdot 10^{15}$ cm^{-2})

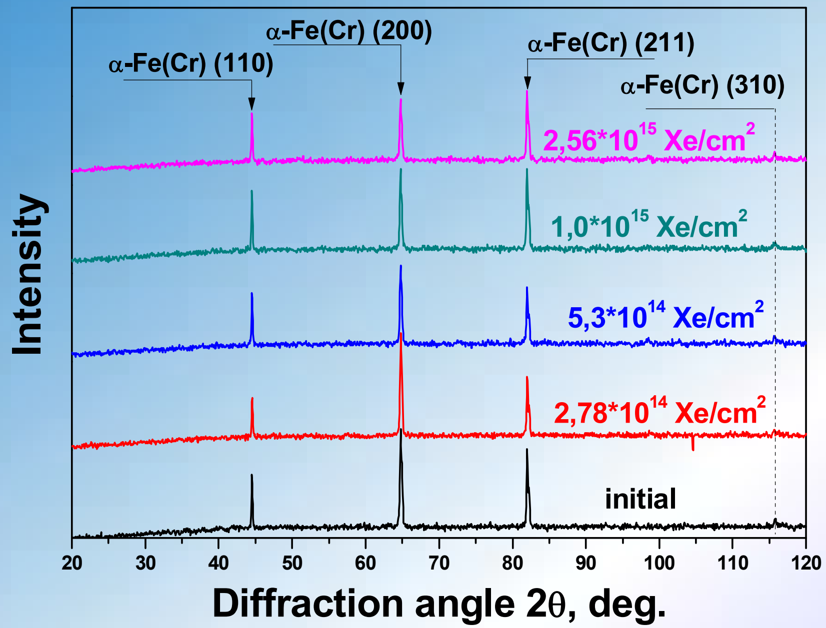

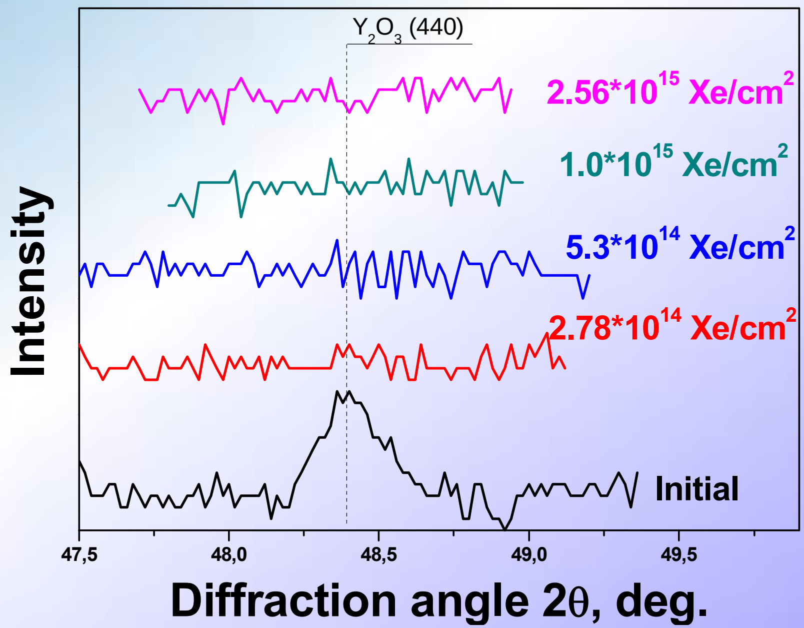

KP-4 + Bi 1.5e13 cm^{-2}

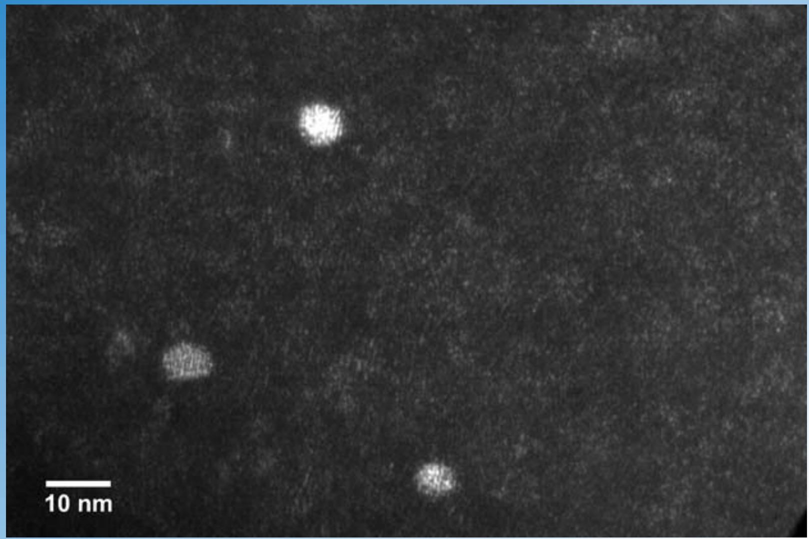

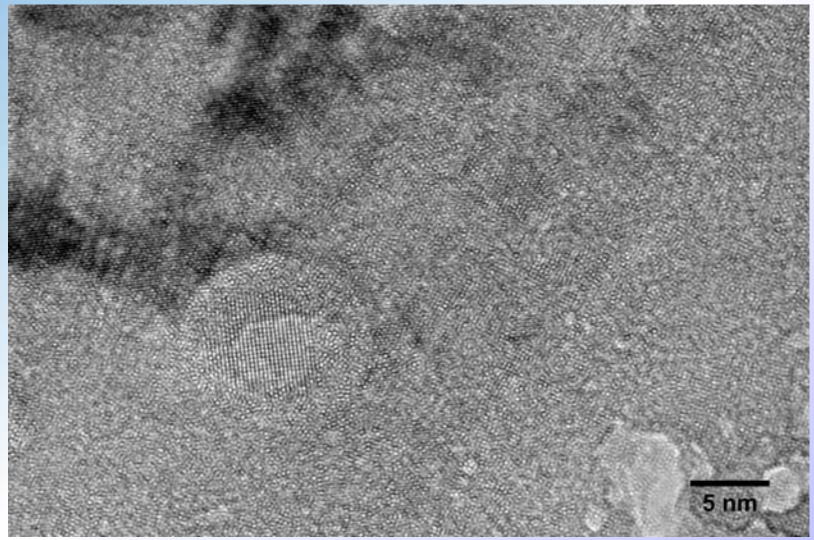

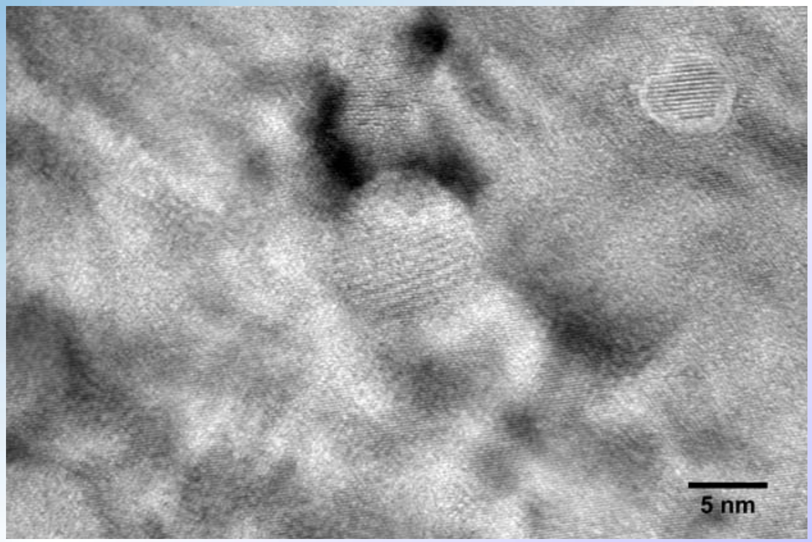

- No oxide nanoparticles dissolution
- Partial amorphization is observed in a large oxide particles. First, periphery of large particles is amorphized. Central regions and small oxides remain crystalline

KP-4 Xe 1.5e15 cm^{-2}

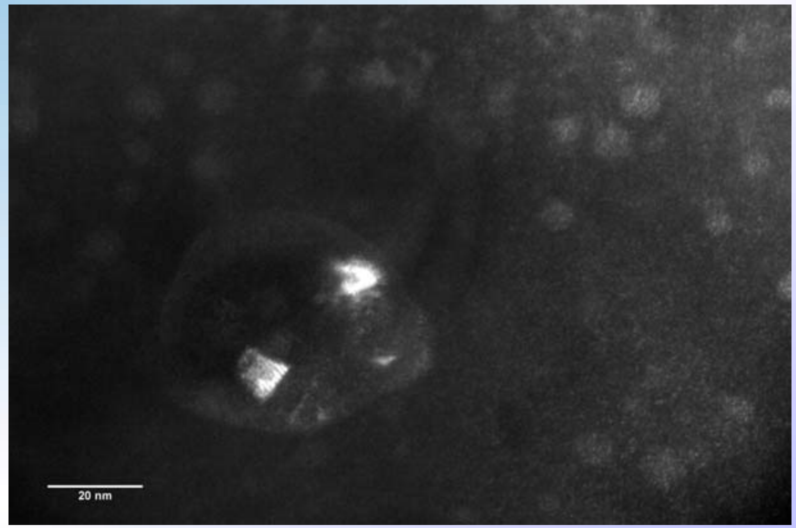

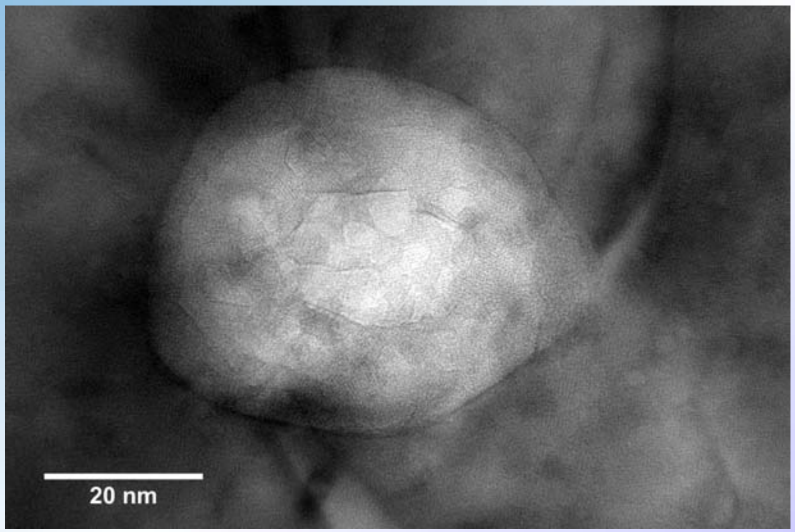

- No oxide nanoparticles dissolution
- Defragmentation of single crystalline oxide particles is observed
- The size of crystalline fragments decreases with ion fluence. Typical size of fragments at 1.5e15 Xe/cm^2 in a large oxides < 5 nm. Small oxide particles at these fluence are fragmented to quasi-amorphous state

Thank you for your attention!